Electron Interactions With C_3F_8

L. G. Christophorou[a] and J. K. Olthoff

Electricity Division, Electronics and Electrical Engineering Laboratory,
National Institute of Standards and Technology, Gaithersburg, Maryland 20899-000ل

To aid the many and diverse applications for which perfluoropropane (C_3F_8) is suited, we critically evaluate and synthesize existing knowledge on electron scattering and electron energy-loss processes for the C_3F_8 molecule, and provide recommendations for the most reliable data. We also draw attention to electron-interaction data that are not presently available, but are needed for modeling the behavior of C_3F_8 in practical uses, especially plasma processing. © *1998 American Institute of Physics and American Chemical Society.* [S0047-2689(98)00205-0]

Contents

[a]Electronic mail: loucas.christophorou@nist.gov

1. Introduction

Perfluoropropane (C_3F_8) is a plasma processing gas.[1-6] It is a replacement for chlorofluorocarbons because it is not harmful to stratospheric ozone. However, like other similar compounds (e.g., CF_4, and C_2F_6) it is a global warming gas. Its global warming potential over a 100-year period is 7000 compared to that of CO_2 taken equal to one and its lifetime in the stratosphere is 2600 years.[7] By comparison, the respective global warming potentials of CF_4 and C_2F_6 are 6500 and 9200,[7] and the respective lifetimes 50 000 and 10 000 years[7-9] (see Roehl et al.[10] for infrared band intensities of C_3F_8 and other perfluorinated compounds in relation to their global warming potentials). Besides plasma processing, perfluoropropane is suitable for other applications. It has good thermal and chemical stability, low toxicity, relatively high vapor pressure, and is transparent to light from the infrared region down to about 1300 Å. The magnitude and energy (or E/N, density-reduced electric field) dependence of its electron attachment rate constant and electron drift velocity make it suitable for possible use in externally sustained diffuse discharge switches,[11-16] especially as the electronegative component in mixtures with buffer gases such as Ar and CH_4.[17] Because of its high dielectric strength, it may find uses as a high voltage insulating gas.[18-20]

TABLE 1. Definition of symbols

Symbol	Definition	Common scale and units
$\sigma_{ab}(\lambda)$	Photoabsorption cross section	10^{-22} m^2
$\sigma_{sc,t}(\varepsilon)$	Total electron scattering cross section	10^{-16} cm^2; 10^{-20} m^2
$\sigma_m(\varepsilon)$	Momentum transfer cross section (elastic)	10^{-16} cm^2; 10^{-20} m^2
$\sigma_{e,diff}(\varepsilon)$	Differential elastic electron scattering cross section	10^{-16} cm^2 sr^{-1}; 10^{-20} m^2 sr^{-1}
$\sigma_{e,int}(\varepsilon)$	Integral elastic electron scattering cross section	10^{-16} cm^2; 10^{-20} m^2
$\sigma_{vib,diff}(\varepsilon)$	Differential vibrational excitation cross section	10^{-16} cm^2 sr^{-1}; 10^{-20} m^2 sr^{-1}
$\sigma_{vib,inel,t}(\varepsilon)$	Total vibrational inelastic electron scattering cross section	10^{-16} cm^2; 10^{-20} m^2
$\sigma_{i,part}(\varepsilon)$	Partial ionization cross section	10^{-16} cm^2; 10^{-20} m^2
$\sigma_{i,t}(\varepsilon)$	Total ionization cross section	10^{-16} cm^2; 10^{-20} m^2
$\sigma_{diss,t}(\varepsilon)$	Total dissociation cross section	10^{-16} cm^2; 10^{-20} m^2
$\sigma_{a,t}(\varepsilon)$	Total electron attachment cross section	10^{-17} cm^2; 10^{-21} m^2
$\sigma_{da,t}(\varepsilon)$	Total dissociative attachment cross section	10^{-17} cm^2; 10^{-21} m^2
α/N	Density-reduced ionization coefficient	10^{-22} m^2
$(\alpha - \eta)/N$	Effective ionization coefficient	10^{-22} m^2
$(E/N)_{lim}$	Limiting value of E/N	10^{-21} V m^2
η/N	Density-reduced electron attachment coefficient	10^{-22} m^2
$k_{a,t}$	Total electron attachment rate constant	10^{-10} cm^3 s^{-1}
$(k_{a,t})_{th}$	Thermal total electron attachment rate constant	10^{-13} cm^3 s^{-1}
w	Electron drift velocity	10^6 cm s^{-1}
D_T/μ	Transverse electron diffusion coefficient to electron mobility ratio	V
W	Average energy to produce an electron–ion pair	eV

To aid the many and diverse applications for which C_3F_8 is suited, in this paper we review and critically evaluate existing knowledge on electron scattering and electron energy-loss processes for this molecule and draw attention to data that are not presently available, but are needed for modeling the behavior of C_3F_8 in practical uses, especially plasma processing.

As in the previous review papers in this series,[21–24] a number of collision cross sections, coefficients, and rate constants are used in this work to quantify various processes which result from the collisions of low-energy electrons with the C_3F_8 molecule. These are defined in Table 1 along with the corresponding symbols and units.

When possible, "recommended" cross sections and transport coefficients are given using the same criteria and procedure discussed in Christophorou et al.[21] As in the previous four papers of this series,[21–24] the recommended values are derived from fits to the most reliable data that are available at the time of preparation of the article and are not necessarily "final." The reliability of each set of data is determined by the following criteria: (i) data are published in peer reviewed literature; (ii) no evidence of unaddressed errors; (iii) data are absolute determinations; (iv) multiple data sets are consistent with one another over ranges of overlap within combined stated uncertainties; and (v) in regions where both experimentally and theoretically derived data exist, the experimental data are preferred. In instances where only a single set of reliable data for a given cross section or coefficient satisfies the above-mentioned criteria, that set is designated as recommended and is tabulated as originally published. In cases where two or more data sets satisfy the selection criteria, each selected data set is analyzed by a weighted-least-squares (WLS) fit, with the resulting data having an equal spacing of points. This is done in order to

ensure that each selected data set is equally weighted in the final fit regardless of the number of points in the original data. The recommended data set is then derived by a combined WLS fit to all of the data, and is presented in tabular and graphical format. When the above criteria are not satisfied, we either make no recommendation or "suggest" certain data in the absence of recommended values.

The cross sections and rate coefficients that are discussed in this paper are based on independently evaluated data. They are not model dependent. They are useful as known inputs to modeling codes, but they do not necessarily constitute a "complete set" for such computations.

2. Electronic and Molecular Structure

The C_3F_8 molecule is nonpolar. Beran and Kevan[25] reported the values of 73.6×10^{-25}, 94.0×10^{-25} and 64.7×10^{-25} cm^3 for the static polarizability of C_3F_8 depending on the method of calculation they used. The absence of electron–electric dipole scattering has a rather profound effect on the electron scattering cross section at low energies (< 1 eV) in comparison to polar gases, as can be seen from the data on the total electron scattering cross section presented later in the paper.

A rather limited number of photoelectron and photoabsorption studies have been made for this molecule. In a mass spectrometric study of the photoionization of C_3F_8, Noutary[26] found no parent positive $C_3F_8^+$ ions. He determined photoionization thresholds for the production of $C_3F_7^+$, $C_2F_5^+$, and CF_3^+ which are listed in Table 2. Robin[27] reported an overall value of the photoionization onset equal to 13.70 eV based on photoelectron spectra. From studies on the photoelectron spectra of the perfluoroalkane molecules,

TABLE 2. Ionization threshold energies for C_3F_8

Ionization threshold (eV)	Ion	Method	Ref.
13.38		Photoelectron spectroscopy	29
13.70			27
15.44±0.02	$C_3F_7^+$ [a]	Photoionization	26
13.32±0.02	$C_2F_5^+$	Photoionization	26
13.22±0.02	CF_3^+	Photoionization	26
13.3±0.1		Electron impact	33
23.5	F^+	Electron impact	49
21.0	CF^+		35
26.6	CF_2^+		35
13.4±0.1 [b]	CF_3^+	Electron impact	79
14.65 [c]			49
14.4 [c]			30
14.70 [c]			77
15.2 [d]			35
13.5±0.1 [b]	$C_2F_4^+$	Electron impact	79
14.4 [d]			35
13.9±0.1 [b]	$C_2F_5^+$	Electron impact	79
15.25 [c]			49
15.3 [c]			30
15.3 [d]			35
15.7±0.1 [b]	$C_3F_7^+$	Electron impact	79
16.5 [c]			49
17.0 [c]			77
17.1 [c]			30
15.5			35

[a] Reaction identified as $C_3F_8 + h\nu \rightarrow C_3F_7^+ + F + e$.
[b] Use was made of the retarding potential difference (RPD) method to improve the electron beam energy resolution.
[c] No RPD was used; inferior electron beam energy resolution.
[d] Possibly high due to poor electron beam energy resolution.

he concluded that the uppermost molecular orbitals (MOs) in these systems are C–C σ–MOs and that for C_3F_8 the transitions from these MOs to $3s$ orbitals (B bands) can be seen as weak excitations at 9.51 eV. The absorption spectrum of the C_3F_8 molecule has been measured by Bélanger et al.[28] in the gas phase for pressures varying from 13.3 to 66.7 Pa. This is reproduced in Fig. 1. It is structureless and peaks at 1190 Å
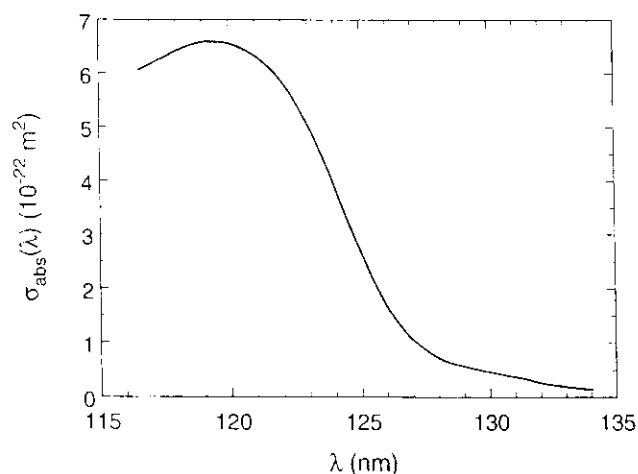
FIG. 1. Photoabsorption spectrum of C_3F_8 (from Bélanger et al., Ref. 38).

(10.42 eV). The value of the absorption cross section at this wavelength is $\sim 6.6 \times 10^{-22}$ m^2.

Absolute oscillator strength spectra for C_3F_8 in the C $1s$ (280–340 eV) and F $1s$ (680–740 eV) regions have been determined by Ishii et al.[31] from inner-shell electron energy-loss spectra using 2.5 keV energy electrons and scattering angles less than 2°. These investigators also measured the electron transmission spectrum of C_3F_8 and found negative ion resonances at 3.34 and 6.00 eV. They attributed these to σ^* molecular orbitals, since the molecule is saturated and the resonances are located well below the region in which the lowest Feshbach resonances are expected. The values they measured are in reasonable agreement with those determined from electron attachment, electron scattering, and vibrational excitation cross section experiments (Table 3; also, Sec. 6 later in the paper). The energy positions of the negative ion resonances as determined from electron scattering experiments should lie at somewhat higher energy than the energy positions determined from dissociative electron attachment studies due to the effects of autodetachment on the competition between dissociation and autodetachment. From the data in Table 3, it can be concluded that there are at least three negative ion states for the C_3F_8 molecule at about 3.5, 6.4, and 9.0 eV (these values are the averages of the electron scattering and electron transmission data in Table 3). Their effects are prominently shown in the cross sections for electron scattering from the C_3F_8 molecule at energies below about 10 eV (Sec. 3).

Perfluoropropane is an electron attaching gas. It forms dissociative attachment fragment anions via a number of resonances lying mostly in the energy range 2–7 eV, and, in addition, it forms parent negative ions via a low lying negative ion state which is attractive and which although short-lived (lifetime $< 10^{-10}$ s) can be stabilized via collisions in high-pressure experiments.[32] The most abundant dissociative attachment fragment negative ion is F^-. Interesting temperature dependencies have been observed[32,33] which show that the production of parent anions decreases[32] and the production of fragment anions increases[32,33] with increasing gas temperature.

There is evidence for direct vibrational excitation at low energies (< 1 eV) and strong indirect vibrational excitation via resonances in the energy range of about 2–10 eV. Similar to the case of CF_4 and C_2F_6, excitation of C_3F_8 to any electronic or ionic state results in fragmentation[34] and consequently, the measured dissociation cross section for C_3F_8 is the sum of the cross sections for all these processes. The most abundant fragment positive ion is CF_3^+.[35]

3. Electron Scattering

In this section information is presented and discussed on the following cross sections: total electron scattering cross section $\sigma_{sc,t}(\varepsilon)$, momentum transfer cross section (elastic) $\sigma_m(\varepsilon)$, differential elastic electron scattering cross section $\sigma_{e,diff}(\varepsilon)$, integral elastic electron scattering cross section $\sigma_{e,int}(\varepsilon)$, differential vibrational excitation cross section

TABLE 3. Energies of negative ion states of C_3F_8

Energy position (eV)	Type of study	Reference
3.9	Total electron scattering	36
6.6		
9.0		
~3	Maximum in calculated $\sigma_m(\varepsilon)$	40
3.2	Peaks in the differential	37[a]
6.5	vibrational electron scattering	
9.0	cross section	
22		
~4.5	Broad peak in the calculated vibrational inelastic scattering cross section	40[b]
3.34	Electron transmission	31[a]
6.00		
1.4	SF_6 scavenger technique[c]	41
~2.0		
~4.0		
2.8	Maximum in total dissociative electron attachment cross section	33
3.3	Maximum in total dissociative electron attachment cross section	77
2.95	Position of dissociative attachment maximum[d]	32
3.15±0.1 (for F⁻)	Dissociative attachment	78
3.65±0.1 (for CF_3^-)		
2.9±0.1 (for F⁻)	Dissociative attachment	71
3.2±0.1 (for $C_2F_5^-$)		
3.3±0.1 (for $C_2F_3^-$)		
3.4±0.1 (for CF_3^-)		
3.75±0.1 (for $C_3F_7^-$)		

[a]Attributed by the authors to shape resonances.

[b]The peak in the calculated vibrational inelastic electron scattering cross section at ~0.7 eV could be attributed to direct vibrational excitation.

[c]This is, in essence, a threshold electron excitation technique (see Ref. 42). The peaks at 1.4 and at 2.0 eV are in conflict with the rest of the data listed in the table and may reflect the fact that some of the scattered electrons which were picked up by SF_6 to form the SF_6^- detected might have been due to direct electron scattering via vibrational excitation rather than scattering from resonances.

[d]The figure given in the table is for 300 K. The position of the resonance decreases with increasing temperature (see Ref. 32 and Sec. 6.6).

$\sigma_{vib,diff}(\varepsilon)$, and vibrational inelastic electron scattering cross section $\sigma_{vib,inel}(\varepsilon)$. The data for all these cross sections are meager, mostly single-set measurements or calculations. The calculated data are especially uncertain. For $\sigma_{sc,t}(\varepsilon)$ the cross section data of Sanabia et al.[36] are recommended. The cross section data of Shinohara et al.[37,38] for $\sigma_m(\varepsilon)$, $\sigma_{e,diff}(\varepsilon)$, and $\sigma_{e,int}(\varepsilon)$ are suggested.

A recent set of cross sections obtained by Jeon and Nakamura[39] based upon multi-term Boltzmann code calculations compared with measurements they made of the electron swarm drift velocities and the product of gas number density and longitudinal electron diffusion coefficient in C_3F_8–Ar mixtures are preliminary and are not presented in this paper.

3.1. Total Electron Scattering Cross Section, $\sigma_{sc,t}(\varepsilon)$

In Fig. 2 are shown the total electron scattering cross section measurements of Sanabia et al.[36] To our knowledge this
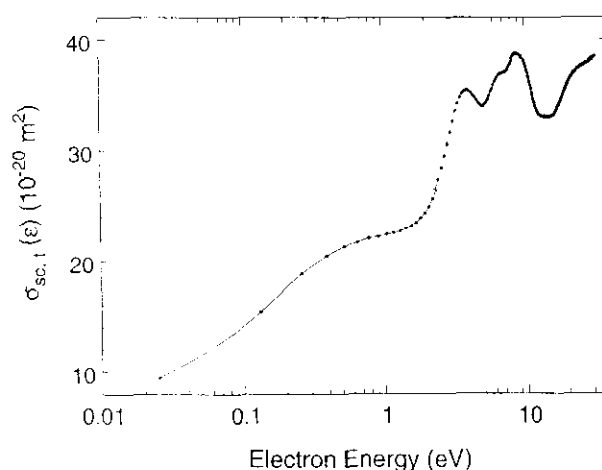
FIG. 2. Total electron scattering cross section, $\sigma_{sc,t}(\varepsilon)$, for C_3F_8 (measurements of Sanabia et al., Ref. 36).

set of measurements is the only one available to date. No calculated values of this quantity have been reported. The cross section has a shoulder at about 0.8 eV, and three maxima at about 3.9, 6.6, and 9.0 eV. These maxima are due to indirect electron scattering via the negative ion states of C_3F_8 at these energies, as has also been indicated by other studies (Table 3). The $\sigma_{sc,t}(\varepsilon)$ in Fig. 2 declines for energies below about 0.8 eV as the electron energy approaches zero due probably to the presence of a Ramsauer–Townsend minimum at these low energies. The calculations of Pirgov and Stefanov[40] indicate such a minimum in the momentum transfer cross section $\sigma_m(\varepsilon)$ at about 0.07 eV (Sec. 3.2.). The existence of a Ramsauer–Townsend minimum would be consistent with the behavior of $\sigma_{sc,t}(\varepsilon)$ for CF_4 and C_2F_6 and would imply that $\sigma_{sc,t}(\varepsilon)$ for C_3F_8 should increase as the electron energy approaches 0 eV.

The region between 0.2 and 2 eV shows an enhancement in the scattering cross section which may be due to direct vibrational excitation. This would be consistent with the peak around 0.7 eV in the vibrational inelastic electron scattering cross section calculated by Pirgov and Stefanov[40] (Sec. 3.6.). It would also be consistent with the broad features of the threshold-electron excitation spectrum of C_3F_8 reported by Lifshitz and Grajower.[41] In this threshold electron excitation technique,[42] SF_6 is mixed with C_3F_8 and the SF_6^- current is monitored as a function of the electron energy. The SF_6^- ions are presumed to be formed by capture of thermal (or near thermal energy) electrons generated in collisions of fast electrons with C_3F_8 which have lost "all" of their energy to excitation of the molecule. The yield of SF_6^- versus electron energy then should exhibit maxima at energies corresponding to the positions of the negative ion states of C_3F_8, since electrons having kinetic energies equal to the resonance energies can lose all of their energy in a single collision and be slowed down to "zero" energy where they are captured efficiently by SF_6 forming SF_6^-. The SF_6^- threshold electron excitation spectrum reported by Lifshitz and Grajower[41] showed a "narrow resonance" at 1.4 eV and a broad peak with maximum intensity at ~2 eV (it also indicated a weak enhancement at ~4 eV). It would seem that since no other technique showed a resonance at 1.4 eV, the observation of Lifshitz and Grajower may reflect the fact that some of the scattered electrons which were picked up by SF_6 might have been due to direct electron scattering due to vibrational excitation rather than indirect scattering from resonances. This would be consistent with the results of Sanabia et al.[36] which indicate direct vibrational excitation below 2 eV, and with the low lying maximum in the calculated[40] $\sigma_{vib,inel}(\varepsilon)$ (Sec. 3.6.). This, in turn, may indicate that experiments which rely on threshold-electron detection for the location of negative ion states of molecules may be in error when the negative ion states are located in an energy range where thermal electrons are also produced efficiently by inelastic scattering via nonresonant processes.

The cross sections of Sanabia et al.[36] are listed in Table 4 as our recommended data for the total scattering cross section of C_3F_8.

TABLE 4. Recommended total electron scattering cross section, $\sigma_{sc,t}(\varepsilon)$, for C_3F_8 [a]

Energy (eV)	$\sigma_{sc,t}(\varepsilon)$ (10^{-20} m^2)	Energy (eV)	$\sigma_{sc,t}(\varepsilon)$ (10^{-20} m^2)
0.025	9.43	0.90	22.3
0.030	9.98	1.0	22.4
0.035	10.4	1.5	23.1
0.040	10.9	2.0	24.5
0.050	11.6	2.5	27.6
0.060	12.2	3.0	31.7
0.070	12.8	3.5	34.8
0.080	13.3	4.0	35.4
0.090	13.7	5.0	34.0
0.10	14.2	6.0	36.0
0.15	16.1	7.0	37.0
0.20	17.6	8.0	37.9
0.25	18.7	9.0	38.7
0.30	19.5	10.0	37.8
0.35	20.1	12.5	33.3
0.40	20.5	15.0	33.0
0.50	21.2	20.0	35.9
0.60	21.6	25.0	37.5
0.70	21.9	30.0	38.2
0.80	22.1	32.0	38.5

[a]Measurements of Sanabia et al., Ref. 36.

3.2. Momentum Transfer Cross Section (Elastic), $\sigma_m(\varepsilon)$

There has been one unpublished, experimental determination of the momentum transfer cross section, $\sigma_m(\varepsilon)$, for C_3F_8 based on differential elastic electron scattering cross section measurements for this molecule.[37,38,43] Shinohara et al.[37] determined their momentum transfer cross sections from the differential elastic electron scattering cross sections they measured (see Fig. 4 in Sec. 3.3.) after extrapolation to the full angle range by modified phase-shift fitting. Their data (provided by Professor Tanaka[38]) are plotted in Fig. 3.

This experimentally based cross section is compared with the momentum transfer cross section for the C_3F_8 molecule calculated by Pirgov and Stefanov.[40] The calculations are Boltzmann type and are based on measured values of the electron drift velocity, w, and transverse electron diffusion coefficient to mobility ratio D_T/μ as a function of E/N in pure C_3F_8 and in mixtures of C_3F_8 with argon. Pirgov and Stefanov used the w and D_T/μ of Naidu and Prasad[45] for pure C_3F_8 in the range $270 \times 10^{-21} - 600 \times 10^{-21}$ V m^2, and the data of Hunter et al.[16] for pure C_3F_8 in the range 0.1 $\times 10^{-21} - 200 \times 10^{-21}$ V m^2. They also used the w data of Hunter et al.[16] for mixtures of C_3F_8 with Ar or CH_4 and dissociative electron attachment cross section of C_3F_8. For the elastic momentum transfer cross section of argon they used the data of Milloy et al.[46] and Spencer and Phelps.[47] Besides the distinct minimum in the momentum transfer cross section at about 0.07 eV, the $\sigma_m(\varepsilon)$ values of Pirgov and Stefanov show a maximum at about 3 eV due to negative ion resonances. The position of the maximum at 3 eV compares well with other data on electron scattering and electron attachment (see Table 3).
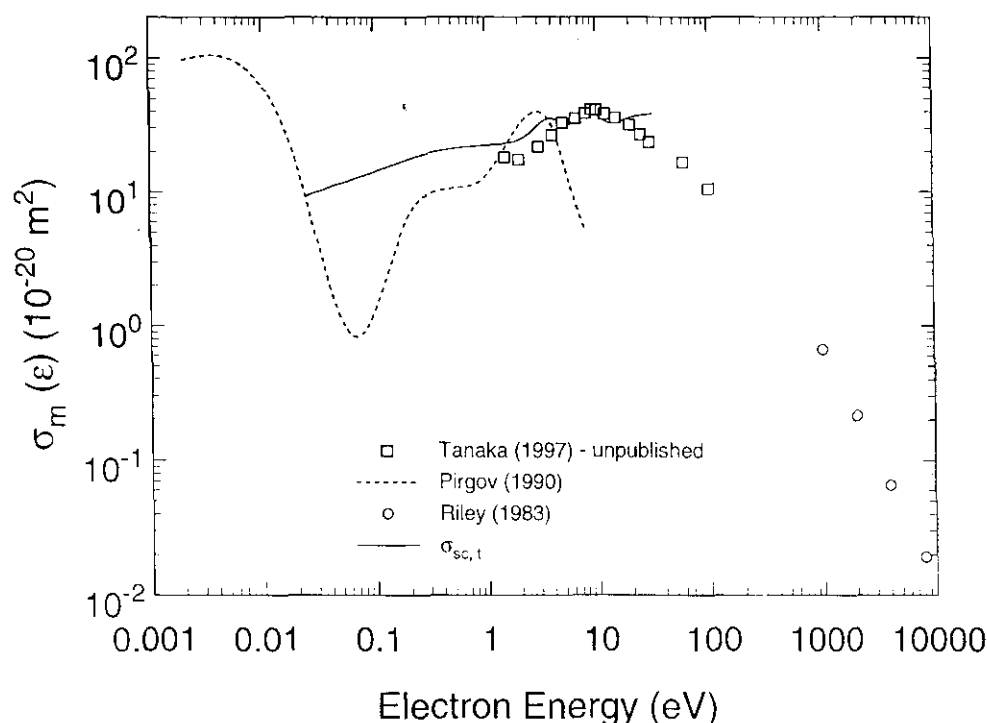
FIG. 3. Momentum transfer cross section (elastic), $\sigma_m(\varepsilon)$, for C₃F₈: (□) Refs. 37 and 38; (○) Ref. 48; (---) Ref. 40. The solid line (—) is the total electron scattering cross section, $\sigma_{sc,t}(\varepsilon)$, from Fig. 2, plotted here for comparison purposes.

There has also been an independent model calculation of $\sigma_m(\varepsilon)$ within the Born approximation by Riley et al.[48] The results of this calculation cover the energy range from 1 to 8 keV. As seen from Fig. 3, these calculated high-energy values of $\sigma_m(\varepsilon)$ are consistent with the measurements of Shinohara et al.[37] and help establish the high energy asymptotic values of σ_m.

The total electron scattering cross section $\sigma_{sc,t}(\varepsilon)$ of Sanabia et al.[36] is also shown in Fig. 3 for comparison purposes. The difference between $\sigma_{sc,t}(\varepsilon)$ and $\sigma_m(\varepsilon)$ below 3 eV may reflect the effect of the vibrational excitation cross section. We list in Table 5 the data of Shinohara et al.[37] from Fig. 3 as our suggested values for the $\sigma_m(\varepsilon)$ of C₃F₈.

3.3. Differential Elastic Electron Scattering Cross Section, $\sigma_{e,diff}(\varepsilon)$

Figure 4 shows the differential elastic electron scattering

TABLE 5. Momentum transfer (elastic) cross section, $\sigma_m(\varepsilon)$, for C₃F₈ [a]

Energy (eV)	$\sigma_m(\varepsilon)$ $(10^{-20}\ m^2)$	Energy (eV)	$\sigma_m(\varepsilon)$ $(10^{-20}\ m^2)$
1.5	18.2	10.0	41.0
2.0	17.5	12.0	38.3
3.0	21.9	15.0	35.8
4.0	26.7	20.0	31.8
5.0	33.0	25.0	27.0
6.5	35.2	30.0	23.6
8.0	38.7	60.0	16.7
9.0	41.3	100.0	10.5

[a]Data of Shinohara et al., Refs. 37 and 38.

cross section, $\sigma_{e,diff}(\varepsilon)$, of the C₃F₈ molecule as measured by Shinohara et al.[37,38] for incident electron energies ranging from 2 to 100 eV and for scattering angles between 30° and 130°. They determined the absolute values of the elastic differential electron scattering cross sections by reference to those of helium. Figure 4 also shows similar unpublished data of Merz and Linder.[43] These were made at lower values of the incident electron energy (0.4–8.2 eV). A final analysis of these data to calculate values of $\sigma_m(\varepsilon)$ and $\sigma_{e,int}(\varepsilon)$, as in the cases of CF₄ and C₂F₆, has not yet been completed by Merz and Linder.[43] However, the overall agreement between these two measurements of $\sigma_{e,diff}(\varepsilon)$ is reasonable for the overlapping energies.

3.4. Integral Elastic Electron Scattering Cross Section, $\sigma_{e,int}(\varepsilon)$

Shinohara et al.[37,38] extrapolated the differential elastic electron scattering cross sections they measured in the scattering angle range 20° and 130° to 0° and 180°. By modified phase-shift fitting and by proper integration they determined the integral elastic electron scattering cross sections plotted in Fig. 5. These data for $\sigma_{e,int}(\varepsilon)$ are listed in Table 6 as our suggested values.

In Fig. 5 are also shown the high energy (1–8 keV) calculated values of $\sigma_{e,int}(\varepsilon)$. These are independent model calculation results[48] within the Born approximation. They provide high-energy asymptotic limit values for $\sigma_{e,int}(\varepsilon)$.
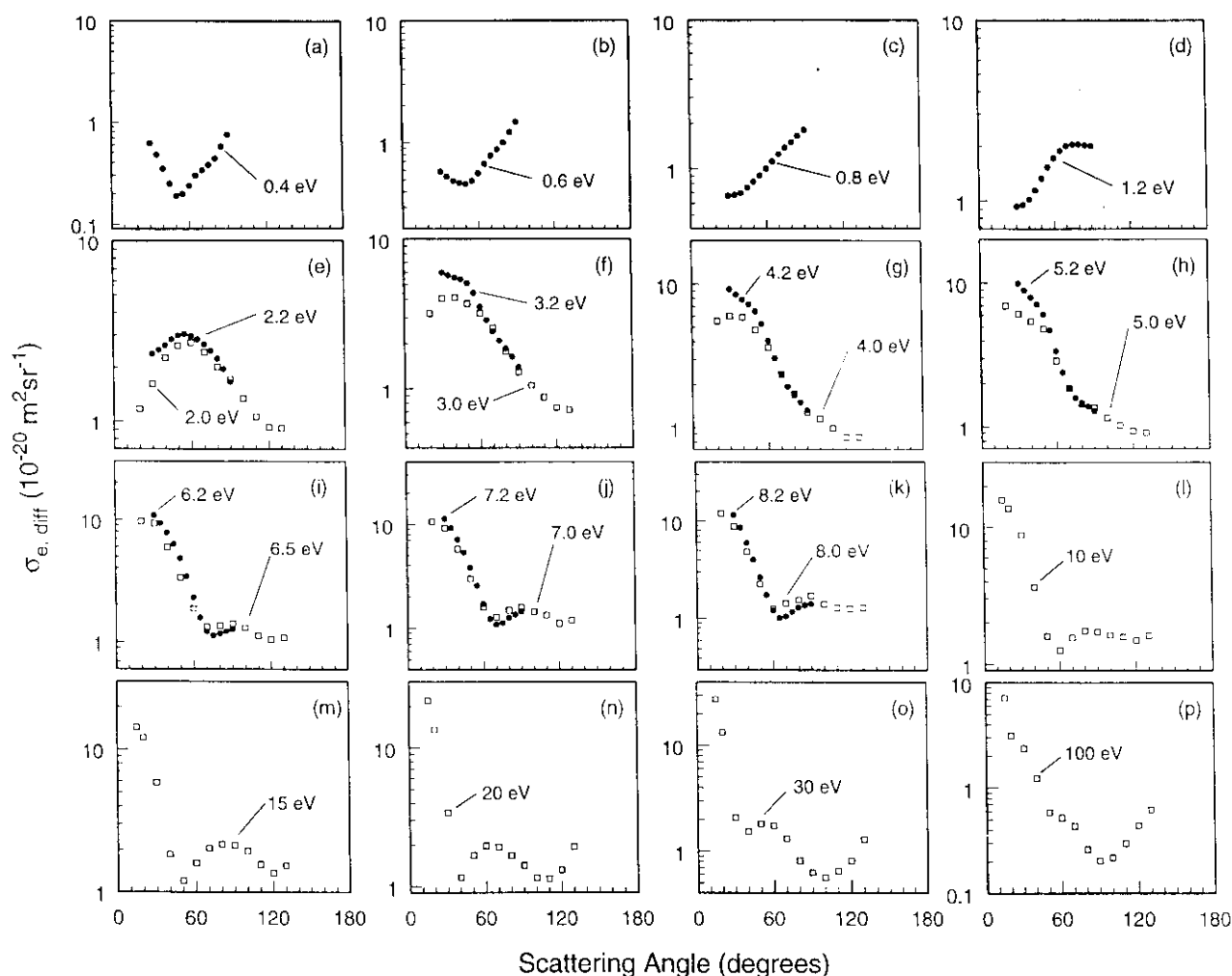
FIG. 4. Differential elastic electron scattering cross section, $\sigma_{e,diff}(\varepsilon)$, for C_3F_8: (□) Experimental data of Shinohara and co-workers, Refs. 37 and 38; (●) Experimental data of Merz and Linder, Ref. 43 (for phase-shift analysis fits to such data, see Ref. 44).

3.5. Differential Vibrational Excitation Cross Section, $\sigma_{vib,diff}(\varepsilon)$

Figure 6 shows the energy dependence of the differential vibrational excitation cross section, $\sigma_{vib,diff}(\varepsilon)$ for the unresolved composite modes at 0.160 eV for a 60° scattering angle as measured by Shinohara et al.[37,38] The cross section shows peaks at 3.2, 6.5, 9.0, and 22 eV, which the authors attributed to shape resonances. The positions of the first three resonances agree well with those determined by other methods (Table 3).

3.6. Total Vibrational Inelastic Electron Scattering Cross Section, $\sigma_{vib,inel,t}(\varepsilon)$

No experimental data are available. A Boltzmann code calculation[40] of the total inelastic vibrational excitation cross section as a function of electron energy is shown in Fig. 7. As with all Boltzmann-derived cross section sets, these data are model dependent and must be considered with caution for use individually. Nonetheless, they show the large vibrational excitation peak at about 4 eV due to indirect scattering

and a peak at about 0.7 eV. The former feature is consistent with the data in Fig. 5 and the shift to higher energy of the inelastic cross section compared to the peak in the momentum transfer cross section. As noted in Sec. 3.1, the latter feature (the peak at 0.7 eV) might be due to direct vibrational excitation since no resonance states have been predicted or observed in this low-energy range. It could explain certain features in the threshold electron excitation spectrum of C_3F_8 observed earlier (Sec. 3.1.).

4. Electron-Impact Ionization

4.1. Partial Ionization Cross Sections, $\sigma_{i,part}(\varepsilon)$

Poll and Meichsner[35] measured the partial ionization cross sections for CF^+, CF_2^+, CF_3^+, $C_2F_4^+$, $C_2F_5^+$, and $C_3F_7^+$ produced by electron impact on C_3F_8 by electrons having kinetic energies in the range of 12.8 to about 130 eV. The CF_3^+ ion has the largest cross section of all six fragment positive ions. We digitized the data of Poll and Meichsner from the graphs
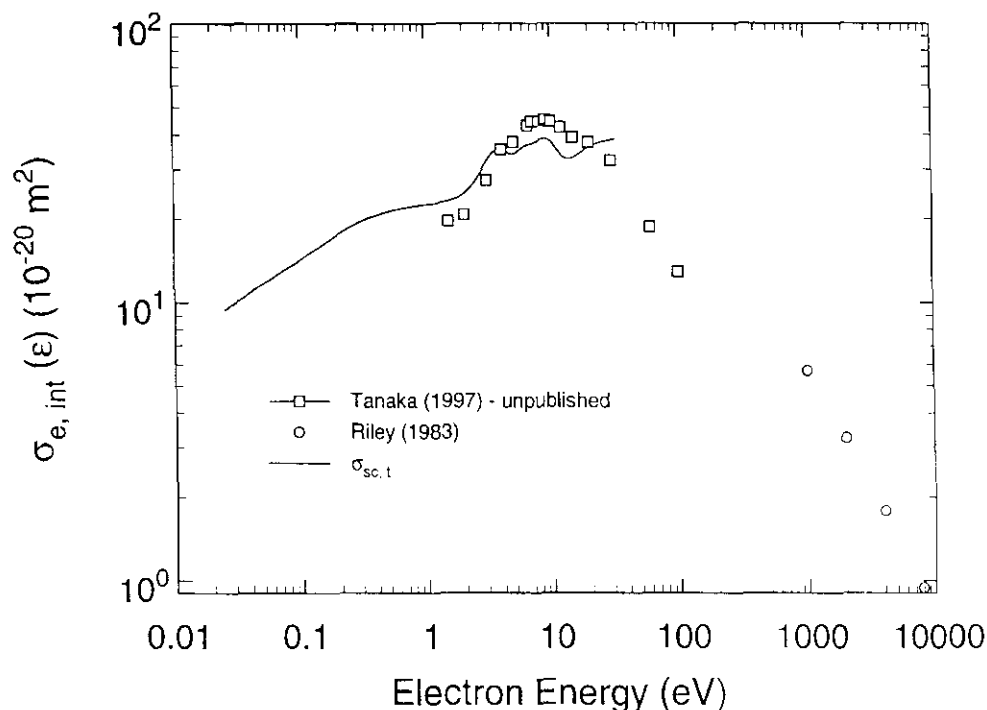
FIG. 5. Integral elastic electron scattering cross section, $\sigma_{e,int}(\varepsilon)$, for C_3F_8: ([]) Refs. 37 and 38; (O) Ref. 48. The solid line (—) is the total electron scattering cross section, $\sigma_{sc,t}(\varepsilon)$, from Fig. 2, plotted here for comparison purposes.

presented in their paper[35] in order to obtain the values listed in Table 7 as our presently suggested values. They are plotted in Fig. 8.

The only other measurement of the partial ionization cross sections for C_3F_8 is that of Bibby and Carter[49] for only one value of the incident electron energy, 35 eV. At this energy, Bibby and Carter measured the cross section for the production of CF_3^+, $C_2F_5^+$, and $C_3F_7^+$, to be, respectively, equal to 1.26×10^{-20}, 0.125×10^{-20}, and 0.16×10^{-20} m^2. These values are, respectively, a factor of 0.35, 0.41, and 0.25 lower than those of Poll and Meichsner.[35]

4.2. Total Ionization Cross Section, $\sigma_{i,t}(\varepsilon)$

There have been five measurements of the total ionization cross section $\sigma_{i,t}(\varepsilon)$ of the C_3F_8 molecule, all of which are shown in Fig. 9. The first was made by Beran and Kevan[50]

for only three values of incident electron energy. These results are shown in Fig. 9 by the ×'s. As we have noted in our earlier papers in this series, the data of Beran and Kevan[50] for a number of small species are generally higher than those of Rapp and Englander-Golden[51] which are generally accepted to be more accurate. The second set of values are those obtained by summation of the partial ionization cross sections measured by Poll and Meichsner[35] (Table 7). These are shown in Fig. 9 by the dashed line. The third measurement was made by Chantry and Chen[33] in the energy range of 13.5 and 80 eV. These workers calibrated their cross section measurements using Xe as the calibrant gas and the total

TABLE 6. Integral elastic electron scattering cross section, $\sigma_{e,int}(\varepsilon)$, for C_3F_8 [a]

Energy (eV)	$\sigma_{e,int}(\varepsilon)$ (10^{-20} m^2)	Energy (eV)	$\sigma_{e,int}(\varepsilon)$ (10^{-20} m^2)
1.5	19.6	9.0	45.0
2.0	20.7	10.0	44.4
3.0	27.4	12.0	42.4
4.0	35.4	15.0	39.1
5.0	37.5	20.0	37.6
6.5	42.9	30.0	32.3
7.0	44.4	60.0	18.7
8.0	44.6	100.0	12.9

[a]Data of Shinohara et al.. Refs. 37 and 38.
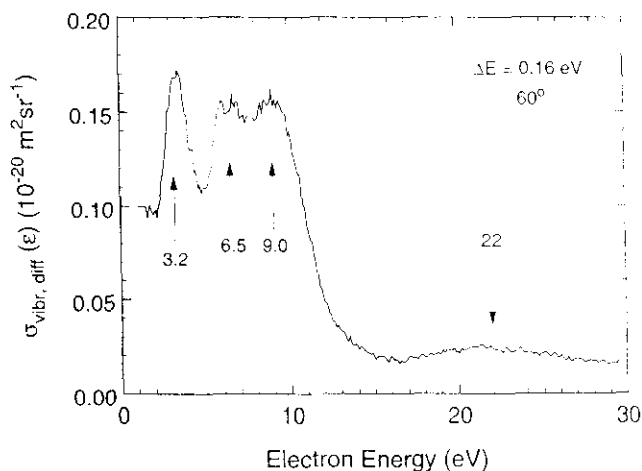
FIG. 6. Differential vibrational excitation cross section, $\sigma_{vibr,diff}(\varepsilon)$, from Ref. 37 for the unresolved composite vibrational modes of C_3F_8 at 160 meV at 60° scattering angle.
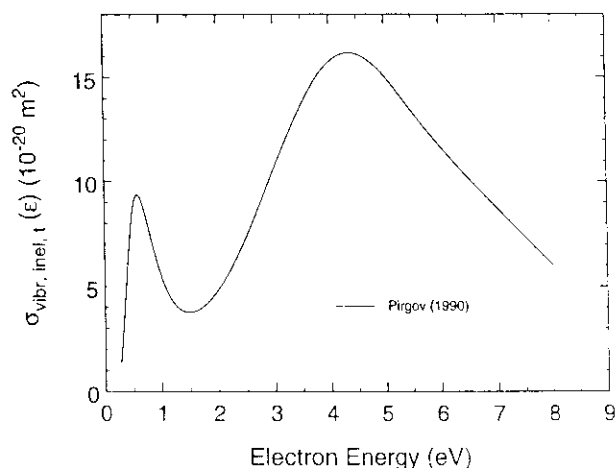
FIG. 7. Total vibrational inelastic electron scattering cross section, $\sigma_{vib,inel,t}(\varepsilon)$, for C_3F_8 (calculated data from Ref. 40).
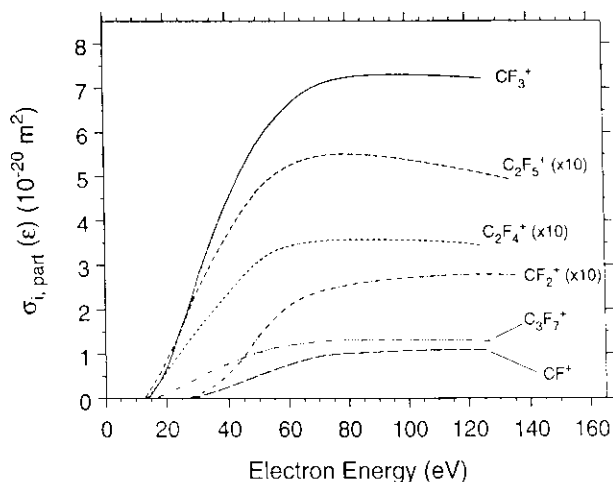
FIG. 8. Partial ionization cross sections, $\sigma_{i,part}(\varepsilon)$, for C_3F_8 (data of Poll and Meichsner, Ref. 35).

ionization cross section for Xe measured by Rapp and Englander-Golden.[51] They reported a total ionization cross section threshold of 13.3 ± 0.1 eV (see ionization threshold values in Table 2). The measurements of Chantry and Chen diverge considerably from other measurements of $\sigma_{i,t}(\varepsilon)$ for C_3F_8, especially at the higher energies they investigated.

A fourth measurement of the absolute determination of $\sigma_{i,t}(\varepsilon)$ for C_3F_8 was recently made by Nishimura et al.[52] These researchers employed a method similar to that of Rapp and Englander-Golden,[51] and claim lower uncertainties ($\sim 7\%$) than the other measurements presented here ($>10\%$). The data of Nishimura et al. are observed to be higher than

the other measurements in Fig. 9, and interestingly their values for this cross section exceed the measured cross section values for total dissociation, $\sigma_{diss,t}(\varepsilon)$, discussed next in Sec. 4.3., for energies greater than 50 eV.

A fifth measurement, as mentioned in the preceding section, is an early report[49] of a measurement of the ionization cross section for the production of the CF_3^+, $C_2F_5^+$, and $C_3F_7^+$ ions from C_3F_8 at one value of the electron energy, namely 35 eV. At this electron energy the sum of the cross sections of Bibby and Carter[49] for the three ions is equal to 1.55×10^{-20} m^2. It is shown in Fig. 9 by the asterisk and is

TABLE 7. Partial ionization cross sections, $\sigma_{i,part}(\varepsilon)$ (in units of 10^{-20} m^2) for C_3F_8 [a]

Energy (eV)	$\sigma_{i,part}(\varepsilon)$ (10^{-20} m^2)					
	CF$^+$	CF$_2^+$	CF$_3^+$	C$_2$F$_4^+$	C$_2$F$_5^+$	C$_3$F$_7^+$
14	....	—	—	...	0.01	....
15	—	--	0.09	0.01	0.02	—
16	....	—	0.19	0.02	0.04	—
17	—	—	0.29	0.03	0.05	0.03
18	—	....	0.40	0.04	0.06	0.05
19	—	...	0.53	0.05	0.07	0.08
20	—	—	0.67	0.06	0.09	0.11
22	—		1.01	0.08	0.11	0.17
24	—	—	1.42	0.10	0.14	0.24
26	—	—	1.80	0.12	0.18	0.31
28	0.01	...	2.19	0.13	0.21	0.38
30	0.04	0.01	2.64	0.15	0.24	0.45
35	0.15	0.03	3.61	0.20	0.31	0.63
40	0.27	0.06	4.45	0.24	0.37	0.78
45	0.41	0.09	5.17	0.28	0.42	0.92
50	0.57	0.14	5.78	0.31	0.47	1.03
60	0.80	0.21	6.59	0.34	0.52	1.19
70	0.96	0.24	7.04	0.35	0.54	1.27
80	1.01	0.26	7.22	0.36	0.55	1.30
90	1.05	0.27	7.29	0.36	0.55	1.31
100	1.07	0.27	7.29	0.36	0.54	1.31
110	1.08	0.28	7.27	0.35	0.53	1.30
120	1.08	0.28	7.23	0.35	0.51	1.29

[a]Data of Poll and Meichsner from Fig. 2(c) of Ref. 35.
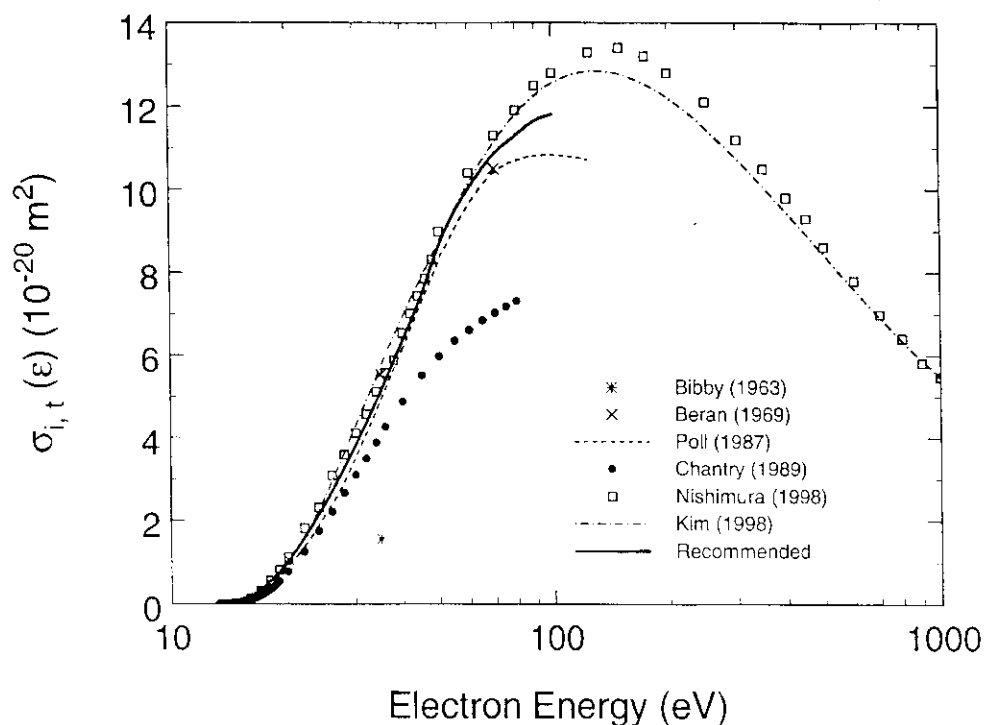
Fig. 9. Total ionization cross section, $\sigma_{i,t}(\varepsilon)$, for C$_3F_8$: (*) Ref. 49; (X) Ref. 50; (---) Ref. 35; (●) Ref. 33; (□) Ref. 52; (−·−) Ref. 52 (calculation); (—) Suggested cross section.

obviously well below the other experimental data.

In view of the fact that the data of Chantry and Chen[33] fall outside of the combined uncertainties when compared with the data of Poll and Meichsner[35] and of Nishimura *et al.*,[52] we have chosen the average of only the latter two sets as our recommended data for $\sigma_{i,t}(\varepsilon)$. However, we have only averaged these data for electron energies up to 100 eV due to the increasing discrepancy between the two measurements at higher energies. The average of these two cross sections is shown in Fig. 9 as a solid line and is tabulated in Table 8.

Figure 9 also shows the recently calculated values of $\sigma_{i,t}(\varepsilon)$ of the C$_3$F$_8$ molecule by Kim and co-workers.[52] Kim's method[53,54] combines binary encounter theory and the Bethe theory of electron impact ionization. The data shown include estimates of multiple ionization, in contrast to earlier calculations on CF$_4$ and C$_3$F$_6$ (see Refs. 21 and 24) by this

method where the contribution to $\sigma_{i,t}(\varepsilon)$ from multiple ionization was not included. Kim's values for C$_3$F$_8$ agree well with the measurements of Nishimura *et al.*[52]

4.3. Total Dissociative Cross Section, $\sigma_{\text{diss},t}(\varepsilon)$

The only available measurement of the total dissociation cross section is that by Winters and Inokuti.[34] This cross section (Fig. 10, Table 9) represents the sum of the cross section for dissociative ionization and the cross section for electron impact dissociation into neutral fragments and has a reported uncertainty of ±20%. The measured values of $\sigma_{\text{diss},t}(\varepsilon)$ are compared in Fig. 10 with the recommended cross section for total ionization (Table 8). Above 70 eV, the recommended values of $\sigma_{i,t}(\varepsilon)$ exceed those of $\sigma_{\text{diss},t}(\varepsilon)$, which is physically impossible but is the result of the relative uncertainties of the measurements.

There are no direct measurements of the cross section for dissociation of the C$_3$F$_8$ molecule into neutral fragments. An estimate of $\sigma_{\text{diss},t}(\varepsilon)$ may be obtained by subtracting the total ionization cross section $\sigma_{i,t}(\varepsilon)$, which is exclusively due to dissociative ionization, from the total dissociation cross section of Winters and Inokuti. This difference is shown in Fig. 10 by the short dashed curve. These values must be considered a gross estimate due to the previously discussed uncertainties in the values suggested for $\sigma_{i,t}(\varepsilon)$ and the relatively large stated uncertainty of $\sigma_{\text{diss},t}(\varepsilon)$. The effect of these uncertainties becomes most apparent at energies above 70 eV, where the recommended values of $\sigma_{i,t}(\varepsilon)$ exceed the measured values of $\sigma_{\text{diss},t}(\varepsilon)$.

TABLE 8. Recommended total ionization cross section, $\sigma_{i,t}(\varepsilon)$, for C$_3F_8$

Energy (eV)	$\sigma_{i,t}(\varepsilon)$ $(10^{-20}$ m$^2)$	Energy (eV)	$\sigma_{i,t}(\varepsilon)$ $(10^{-20}$ m$^2)$
13.0	0.00	30.0	3.81
14.0	0.01	35.0	5.13
15.0	0.06	40.0	6.35
16.0	0.18	45.0	7.46
17.0	0.35	50.0	8.63
18.0	0.56	60.0	10.02
19.0	0.77	70.0	10.85
20.0	1.02	80.0	11.3
25.0	2.42	100.0	11.8

Fig. 10. Total dissociation cross section, $\sigma_{diss,t}(\varepsilon)$, for C_3F_8 (data of Winters and Inokuti, Ref. 34). For compari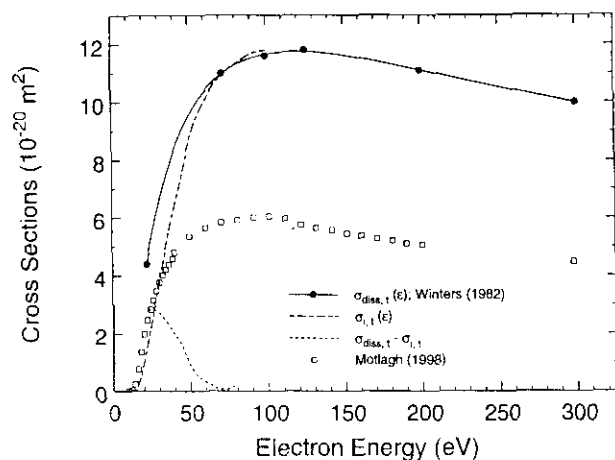son the total ionization cross section $\sigma_{i,t}(\varepsilon)$ (solid curve in Fig. 9) is shown (---) along with the difference (---) $\sigma_{diss,t}(\varepsilon) - \sigma_{i,t}(\varepsilon)$, which is a gross estimate of the cross section for dissociation into neutral fragments. Also shown are the recent measurements of Motlagh and Moore (Ref. 55) on the production of neutral $CF_3 + C_2F_5$ radicals by electron impact on C_3F_8 ($\square$).

Fig. 11. Density-reduced electron impact ionization coefficient, α/N, for C_3F_8: ($\square$) Ref. 59; ($\blacktriangle$) Ref. 45; ($\bullet$) Ref. 60; (—) Recommended value.

Recently, Motlagh and Moore[55] measured the cross section for the production of CF_3 plus C_2F_5 radicals by electron impact on C_3F_8. Their method detects these radicals mass spectrometrically as organotellurides generated upon collision with the surface of a telluride mirror. Their results, which reflect the production of these radicals by both dissociative ionization and by dissociation into neutrals, are also shown in Fig. 10.

The state of excitation of the dissociation fragments is also of considerable interest because it affects the rates of the subsequent reactions of these products and because it produces light which may induce other processes or may be used for diagnostic purposes. Emission bands of CF_3 radicals produced by pulsed electron beam (initial energy 0.6 MeV) excitation have been studied by Hermann,[56] and the formation of excited fragments in collisions of C_3F_8 with electrons having initial energies in the range 0.4–6 keV has been studied by Danilevskii et al.[57] Optical emission spectra of pure C_3F_8 and of C_3F_8–O_2 plasmas have been studied by Chen and Lee.[58] The fluorine emission lines were observed and also emissions from CF_x radicals. For C_3F_8–O_2 plasmas, the relative emission intensity of the fluorine atom and the CF_2 and CF_3 radicals depended on the percentage of O_2 in the mixture (see Ref. 58).

4.4. Ionization Coefficients

4.4.1. Density-Reduced Ionization Coefficient, α/N

There have been three measurements[45,59,60] of the density-reduced ionization coefficient, α/N, as a function of E/N for C_3F_8. These are compared in Fig. 11. Moruzzi and Craggs[59] made measurements at $T = 273$ K and in the E/N range of $273 \times 10^{-21} - 910 \times 10^{-21}$ V m^2. Their data have an estimated uncertainty of $\pm 20\%$.[61] They show some dependence on gas pressure (not evident in Fig. 11) which is not exhibited by the other two sets of measurements. Naidu and Prasad[45] made their measurements at $T = 293$ K, gas pressures in the range of 0.08–0.27 kPa, and E/N values ranging from 273×10^{-21} to 637×10^{-21} V m^2. Their α/N values were found to be pressure independent. They reported an overall uncertainty in their measurements of $\pm 10\%$ at E/N values less than $(E/N)_{lim}$ (see Table 11) and about $\pm 20\%$ at the highest E/N values at which they made measurements. Hunter et al.[60] measured α/N at 298 K in the E/N range $5 \times 10^{-21} - 400 \times 10^{-21}$ V m^2 using a pulsed Townsend technique. The reported uncertainty in their measurements is less than $\pm 10\%$ except when one of the coefficients (electron attachment or ionization) is much smaller than the other. The values of α/N were found to be independent of pressure in the pressure range 0.05 and 20 kPa they investigated. The overall agreement between the three sets of measurements is within the combined uncertainties, although the data of Moruzzi and Craggs are consistently higher than the other two sets of measurements. In view of the higher uncertainty of the earlier measurements, we performed a least squares fit to only the data of Naidu and Prasad[45] and Hunter et al.,[60] which is represented in Fig. 11 by the solid line. Values taken off this curve are listed in Table 10 as our recommended set of data for the electron-impact ionization coefficient, α/N, of C_3F_8.

Table 9. Total dissociation cross section, $\sigma_{diss,t}(\varepsilon)$, for C_3F_8 [a]

Energy (eV)	$\sigma_{diss,t}(\varepsilon)$ (10^{-20} m^2)
22	4.39
72	11.0
100	11.6
125	11.8
200	11.1
300	10.0

[a] Data of Winters and Inokuti, Ref. 34.

TABLE 10. Recommended density-reduced ionization coefficients, α/N, for C$_3$F$_8$

E/N $(10^{-21}$ V m$^2)$	α/N $(10^{-22}$ m$^2)$	E/N $(10^{-21}$ V m$^2)$	α/N $(10^{-22}$ m$^2)$
140	0.12	400	27.8
160	0.99	420	30.7
180	2.02	440	33.9
200	3.34	460	37.7
220	5.02	480	41.7
240	6.88	500	45.4
260	8.84	520	49.0
280	11.1	540	52.9
300	13.4	560	57.3
320	16.2	580	62.0
340	18.9	600	66.6
360	22.1	620	71.3
380	24.9		

4.4.2. Effective Ionization Coefficient $(\alpha - \eta)/N$

Hunter et al.[60] used their data on electron attachment and ionization coefficients to obtain the effective ionization coefficient, $\bar{\alpha}/N = (\alpha - \eta)/N$, over an E/N range above and below the breakdown limit, $(E/N)_{lim}$ (inset of Fig. 12). Although the electron impact ionization coefficient is independent of gas pressure (Sec. 4.4.1.), the electron attachment coefficient increases with increasing pressure over the pres-

sure range investigated by Hunter et al.[60] and thus the effective ionization coefficient should decrease with increasing gas pressure, as is indeed shown by the measurements of Hunter et al. (Fig. 12) and the earlier measurements of Moruzzi and Craggs.[59] One therefore needs to exercise caution when comparisons are made of data from various sources which might have been taken at different pressures. It should also be noted that since the attachment coefficient for C$_3$F$_8$ is also a function of temperature (Sec. 6.6.), one needs to specify the temperature of the system. The measurements of Hunter et al. were made at 298 K and those of Naidu and Prasad and Moruzzi and Craggs at 293 K. For comparison, we have plotted in Fig. 12 the $(\alpha - \eta)/N$ measurements of Moruzzi and Craggs[59] and Naidu and Prasad[45] made at pressures less than 0.133 kPa. There is good agreement between the measurements of Hunter et al.[60] and Naidu and Prasad,[45] but the measurements of Moruzzi and Craggs[59] are higher. The data of Hunter et al. and Naidu and Prasad are preferred.

4.4.3. $(E/N)_{lim}$

The limiting E/N value of an electronegative gas, $(E/N)_{lim}$, is defined as the E/N at which $(\alpha - \eta)/N = 0$. In the absence of significant secondary electron loss or gain processes, $(E/N)_{lim}$ can also be equated with the uniform field high voltage breakdown strength of the gas. As dis-
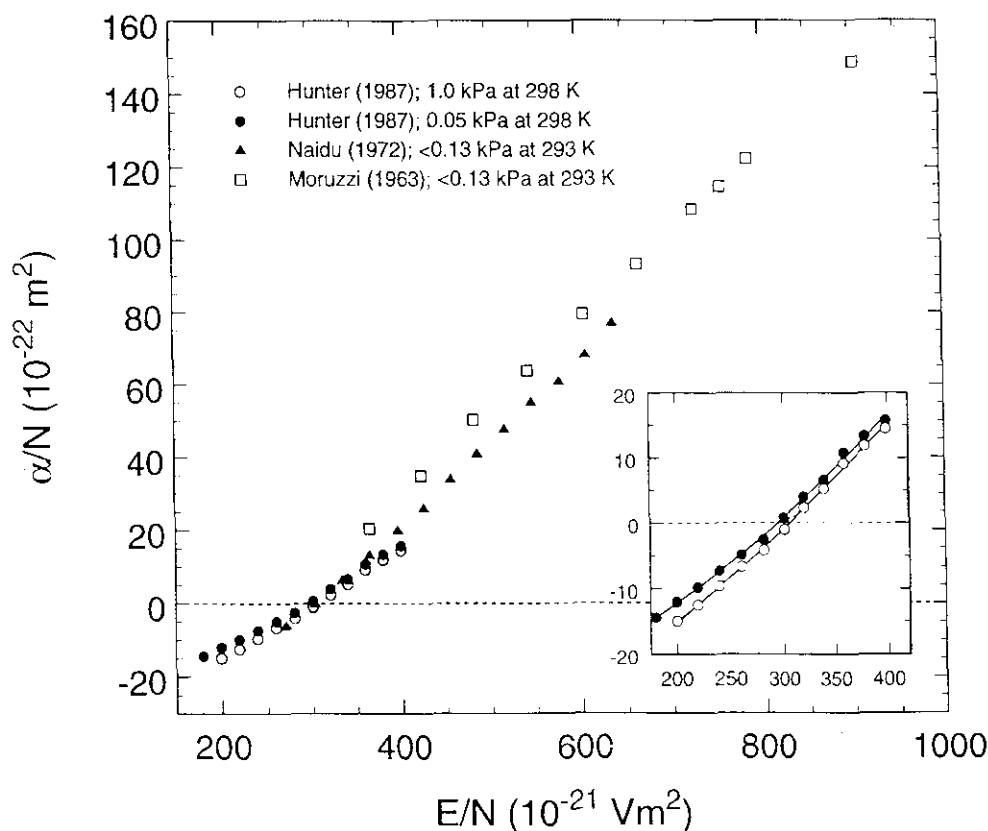

FIG. 12. Effective ionization coefficient, $\bar{\alpha}/N = (\alpha - \eta)/N$, for C$_3F_8$: (○) Ref. 60 ($P = 1.0$ kPa; $T = 298$ K); (●) Ref. 60 ($P = 0.05$ kPa; $T = 298$ K); (▲) Ref. 45 ($P < 0.13$ kPa; $T = 293$ K); (□) Ref. 59 ($P < 0.13$ kPa; $T = 293$ K). Inset graph: Data of Hunter et al. (Ref. 60) for 1.0 and 0.05 kPa, on an expanded scale.

TABLE 11. Values of $(E/N)_{lim}$ for C_3F_8

$(E/N)_{lim}$ (10^{-21} V m^2)	Reference
295–330[a]	60
302–313[b]	45
308[b]	59
317–358[c]	62
331–353[d]	63
353[e]	64
352[f]	19

[a]These values are for the limited pressure range (0.05–2 kPa) employed in Hunter *et al.*, Ref. 60. If it were possible to measure ionization and attachment coefficients at higher pressure, the values of $(E/N)_{lim}$ that would be measured would most likely overlap with the experimental high voltage measurements listed in the table.
[b]Data obtained from low pressure measurements of electron attachment and ionization coefficients.
[c]Breakdown measurements at pressures ranging from 10 to 210 kPa.
[d]Breakdown measurements at pressures ranging from 27 to 285 kPa.
[e]Breakdown measurements at a pressure of 150 kPa.
[f]Breakdown measurements at a pressure of 69.3 kPa.

Fig. 13. Observed variation of the $(E/N)_{lim}$ of C_3F_8 with (a) gas number density (data of Biasiutti, Ref. 62) and (b) temperature (data of Christophorou *et al.*, Ref. 19).

cussed earlier in this section (see also Sec. 6.1.), the electron attachment coefficient of C_3F_8, and hence $(E/N)_{lim}$, are dependent on gas pressure. The latter, therefore, cannot be directly compared with the high voltage breakdown measurements which are usually obtained at atmospheric (or higher) pressures. The data of Hunter *et al.*[60] on $(E/N)_{lim}$ are in good agreement with previous measurements of $(E/N)_{lim}$ based on ionization and attachment coefficients when these measurements were performed over similar pressure ranges[45,59] (Table 11). The values of $(E/N)_{lim}$, obtained from the high voltage breakdown field strength measurements,[62,63] overlap with the values Hunter *et al.* measured at the highest gas pressures they employed (Table 11). At higher pressures, however, the breakdown field measurements give considerably higher $(E/N)_{lim}$ values[62–64] (Table 11). It has been shown[65–67] that the pressure dependence that has been observed in $(E/N)_{lim}$ and in the high voltage breakdown field measurements is due to the pressure dependence of the electron attachment coefficient in this gas and represents a genuine violation of Paschen's law.[66] The variation of $(E/N)_{lim}$ with the C_3F_8 gas density is shown in Fig. 13(a).

Since, moreover, the electron attachment coefficient is a function of the gas temperature, the value of $(E/N)_{lim}$ will vary with gas temperature. Indeed, this has been observed to be so by Christophorou *et al.*[19,68] [Fig. 13(b)]. Finally, measurements have been made of the $(E/N)_{lim}$ of mixtures of C_3F_8 with CH_4 or Ar.[16] Figure 14 shows these measurements.

4.4.4. Average Energy to Produce an Electron-Ion Pair, W

The average energy to produce an electron–ion pair, W, for α particles (initial energy ~5.1 MeV) has been measured by Reinking *et al.*[69] for pure C_3F_8 and found to be 34.4 eV per ion pair. This value is almost identical with those measured by Reinking *et al.* for CF_4 and C_2F_6. They are large compared to the W values of other polyatomic molecules,[42]
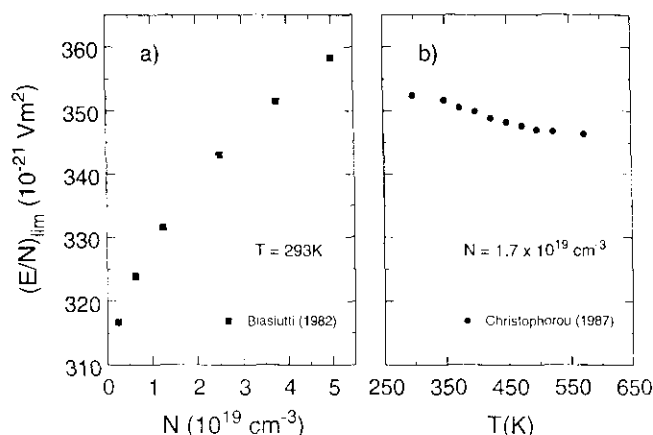
reflecting the high ionization threshold energies for these perfluorocarbon molecules and the considerable amount of energy going into translational and/or internal energy of the fragments that accompany the processes of dissociative ionization in these molecules.

The W values of binary mixtures of C_3F_8 with Ar and C_2H_2 and the ternary mixture C_3F_8–Ar–C_2H_2 have also been measured by Reinking *et al.*[69] Figure 15 shows the W values of the binary mixtures C_3F_8–Ar and C_3F_8–C_2H_2. Interestingly, as noted by Nakanishi *et al.*[70] and Reinking *et al.*[69] the perfluorocarbon-containing gas mixtures show no "Jesse effect," (i.e., an abrupt decrease in the W of the gas mixture as small amounts of C_2H_2 are added to C_3F_8) although a number of excited electronic states of the C_3F_8 molecule exist above the ionization onset of C_2H_2. This has been
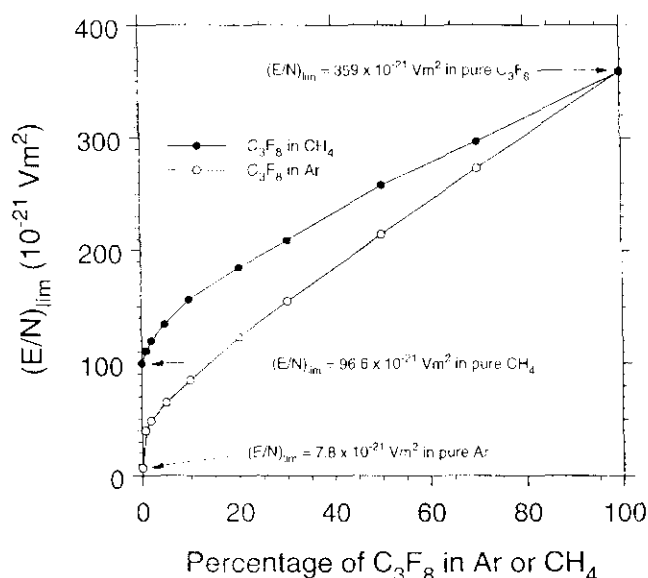
Fig. 14. $(E/N)_{lim}$ as a function of the percentage of C_3F_8 in Ar (O) or CH_4 (●). The total pressure was 109 kPa and the temperature 298 K. The $(E/N)_{lim}$ values for pure Ar, CH_4, and C_3F_8 are shown in the figure (data of Hunter *et al.*, Ref. 16).
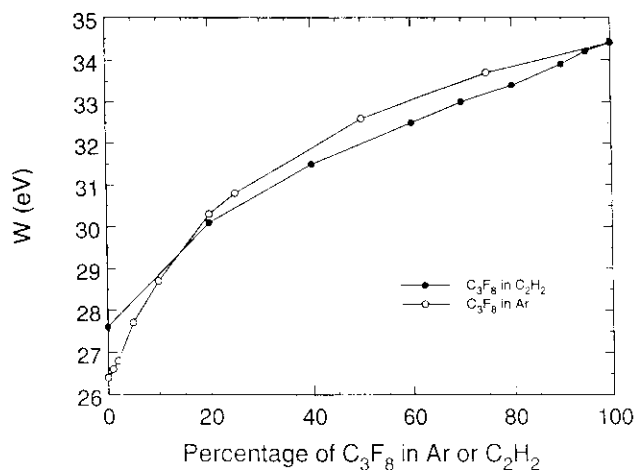
FIG. 15. Average energy needed to produce an electron-ion pair in mixtures of C_3F_8 in Ar or C_2H_2 for α particles (data of Reinking *et al.*, Ref. 69).

FIG. 16. Density-reduced electron attachment coefficient, η/N, for C_3F_8 as a function of E/N at various pressures ($T = 298$ K) (data of Hunter *et al.*, Ref. 60). The broken line refers to the values of η/N at infinite gas pressure.

attributed[69,70] to the fast dissociation of the electronically excited $C_3F_8^*$ molecules.

5. Electron Impact Dissociation Producing Neutrals

No data are available on this process, other than what can be derived from comparisons of $\sigma_{diss,t}(\varepsilon)$ and $\sigma_{i,t}(\varepsilon)$, as discussed in Sec. 4.3.

6. Electron Attachment

6.1. Density-Reduced Electron Attachment Coefficient, η/N

In contrast to CF_4 and C_2F_6, the electron attachment coefficient (and hence the electron attachment rate constant and cross section) of C_3F_8 depends on gas pressure. Electron attachment to CF_4 and C_2F_6 is entirely due to dissociative electron attachment and thus the attachment coefficient for these gases is independent of gas pressure.[32,71] In contrast, at room temperature electron attachment to C_3F_8 is partly due to nondissociative electron attachment producing parent negative ions and partly due to dissociative electron attachment producing fragment negative ions.[32,72] The former are normally collision-stabilized species since the autodetachment lifetimes of the transient parent anion $C_3F_8^{-*}$ are believed to be in the range $10^{-11}-10^{-8}$ s.[32,72]

The pressure dependence of η/N for C_3F_8 is evident in the early η/N measurements[45,59] (not shown here) and is clearly seen in the more recent and detailed results on η/N of Hunter *et al.*[60] reproduced in Fig. 16. The broken curve designated by $P \to \infty$ refers to the value of η/N at "infinite" pressure, that is, when all parent anions are stabilized. The data cover the range of pressure from 0.05 to 10.0 kPa and were taken at 298 K. They have a quoted uncertainty of about $\pm 10\%$ except when one of the coefficients (for electron attachment or ionization) is considerably larger than the other. The data of Naidu and Prasad[45] have an uncertainty
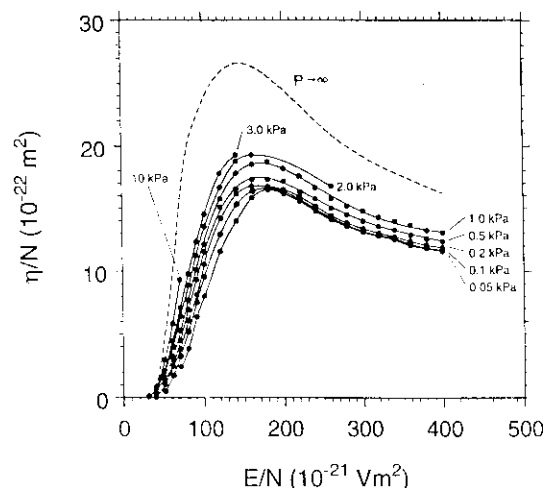
between $\pm 10\%$ at $E/N < (E/N)_{lim}$ and about $\pm 20\%$ at the highest E/N values at which they made measurements. The uncertainty in the measurements of Moruzzi and Craggs[59] is probably $\pm 20\%$.[61] The fact that the η/N for C_3F_8 varies with pressure, makes it difficult to compare its values as measured by various groups. However, the measurements of Naidu and Prasad[45] at 0.22 kPa (at 293 K) can be compared with those of Hunter *et al.*[60] at 0.20 kPa (298 K). This is done in Fig. 17. The data are in agreement within the stated uncertainties.

6.2. Total Electron Attachment Rate Constant, $k_{a,t}$

The density-reduced electron attachment coefficient, $\eta/N(E/N)$, is related to the total electron attachment rate constant, $k_{a,t}(E/N)$, by $k_{a,t}(E/N) = \eta/N(E/N) \times w(E/N)$, where $w(E/N)$ is the electron drift velocity of the unitary gas

FIG. 17. Comparison of the measurements of Hunter *et al.*, Ref. 60 ($T = 298$ K) with those of Naidu and Prasad (Ref. 45) ($T = 293$ K) for the η/N of C_3F_8 taken at about the same pressures: ($\bullet$) 0.20 kPa (Ref. 60); ($\circ$) 0.22 kPa (Ref. 45).
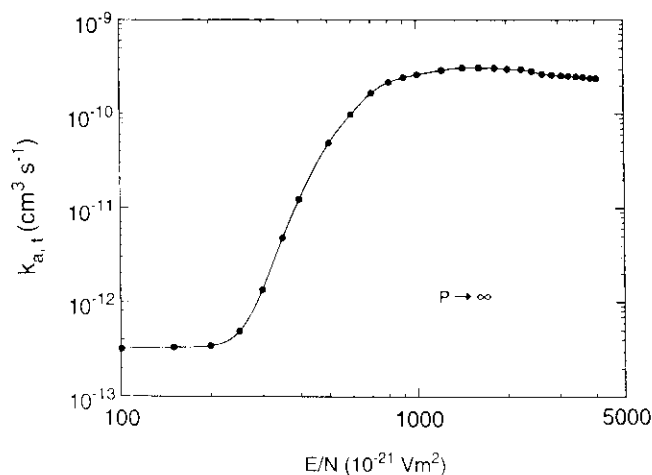
Fig. 18. $k_{a,t}(E/N)$ measured at room temperature in pure C_3F_8 (data of Hunter *et al.*, Ref. 60, extrapolated to infinite total pressure).

(or gas mixture when measurements are made of η/N_a, where N_a is the number density of the electron attaching gas in the mixture). Since $k_{a,t}(E/N)$ depends on gas pressure, care must be taken to specify the number density and the nature of the medium in which the measurement is made, unless the data are extrapolated in some fashion to infinite number density. Measurements have been made of $k_{a,t}(E/N)$ in both pure C_3F_8 and in binary mixtures of C_3F_8 with the buffer gases N_2, Ar, and CH_4. These measurements are presented and discussed below.

6.2.1. $k_{a,t}(E/N)$ Measured in Pure C_3F_8

The only set of measurements of $k_{a,t}(E/N)$ in pure C_3F_8 is that of Hunter *et al.*[60] which is reproduced in Fig. 18. The data shown are the values of the attachment rate constant extrapolated to infinite pressure.[60] They represent the sum of the rate constants for both fragment and parent anions. The data cannot be plotted as a function of mean electron energy because the electron energy distribution functions at the various E/N values employed are not known for pure C_3F_8.

6.2.2. $k_{a,t}(E/N)$ Measured in Binary Mixtures of C_3F_8 with Buffer Gases

There have been three[32,72,73] room temperature measurements of the total electron attachment rate constant of C_3F_8 in argon buffer gas as a function of E/N. These ar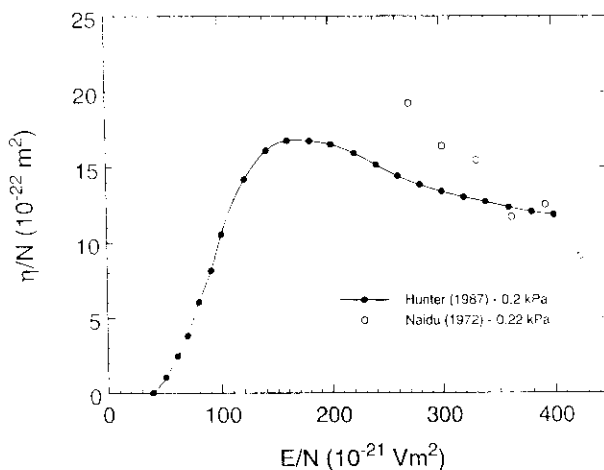e compared in Fig. 19(a). The measurements of Hunter and Christophorou[72] and Spyrou and Christophorou[32] were made over a large E/N range and at a number of buffer gas pressures, in contrast with the data of Wang and Lee[73] which were taken over a limited E/N range and for only one total gas pressure (50.66 kPa). The data sets of Christophorou and coworkers[32,72] plotted in the figure are the values of $k_{a,t}(E/N)$ which were extrapolated to infinite gas pressure. Christophorou and co-workers[32,72] measured $k_{a,t}(E/N)$ as a function of the ratio, R, of the attaching gas to buffer gas pressure, and used the value of $k_{a,t}(E/N)$ extrapolated to $R=0$ so as to correct for the effect of the attaching gas on
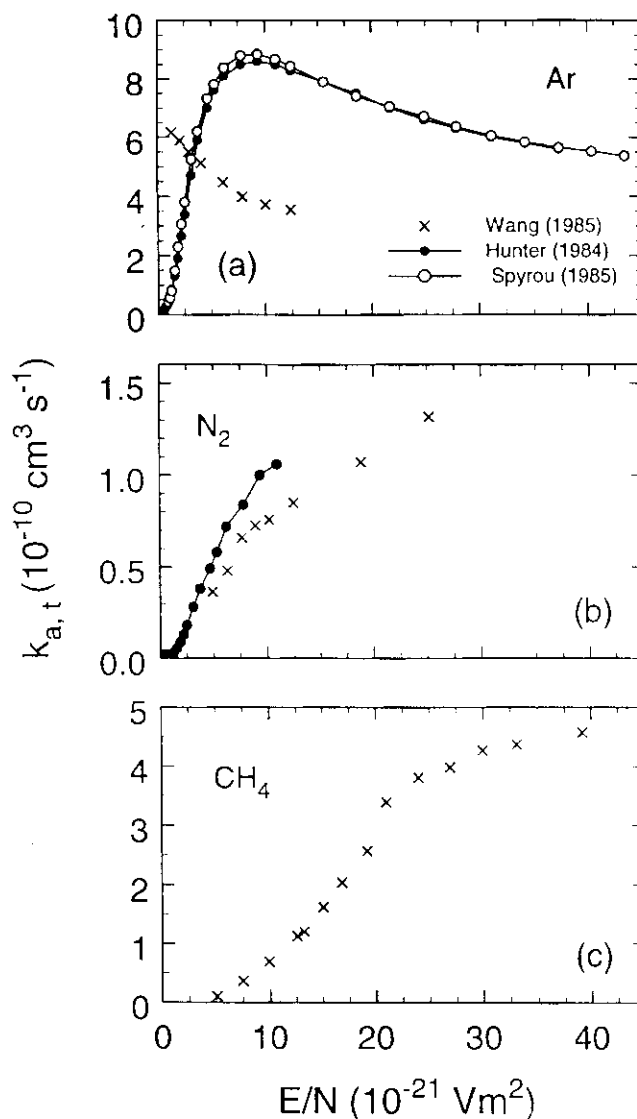
Fig. 19. (a) $k_{a,t}(E/N)$ of C_3F_8 measured at room temperature in mixtures of C_3F_8 with Ar buffer: (●) Ref. 72; (○) Ref. 32; (×) Ref. 73. The data of Refs. 72 and 32 were corrected for both the effect of the C_3F_8 partial and the total gas pressure on the measured rate constants. The data of Wang and Lee (Ref. 73) were corrected only for the former. (b) $k_{a,t}(E/N)$ measured at room temperature in mixtures of C_3F_8 with N_2 buffer: (●) Ref. 72; (×) Ref. 73. The data of Hunter and Christophorou (Ref. 72) were corrected for both the effect of the partial and total pressure on the measured rate constants. The data of Wang and Lee (Ref. 73) were corrected only for the former. (c) $k_{a,t}(E/N)$ measured at room temperature in mixtures of C_3F_8 with CH_4 buffer (×) (data of Wang and Lee, Ref. 73).

the electron energy distribution function of pure argon. Although Wang and Lee[73] mention in their paper that they followed a similar procedure, the large discrepancy between their data and the rest of the measurements in Fig. 19(a) would indicate that the procedure they followed did not entirely compensate for the effect of the attaching gas pressure on the electron energy distribution function in pure argon. While their lower values for the rate constants could be partly due to the fact that their measurements were made at only one buffer gas pressure (and not extrapolated to infinite buffer gas pressure), the difference in the E/N dependence between the Wang and Lee data and those of Christophorou
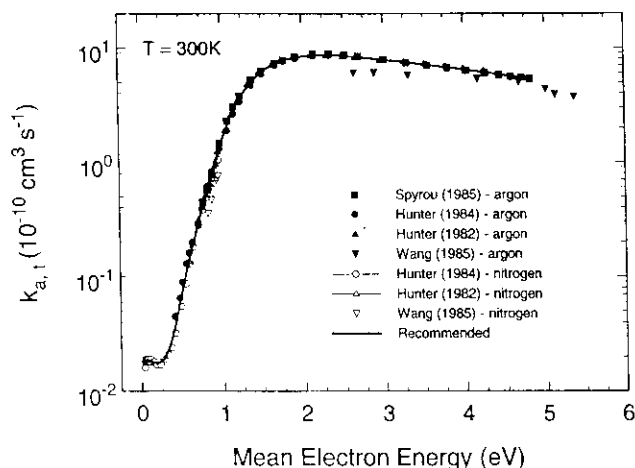
FIG. 20. $k_{a,t}(\langle\varepsilon\rangle)$ for C$_3$F$_8$ ($T = 298$ K). Data from mixtures in Ar: (■) Ref. 32; (●) Ref. 72; (▲) Ref. 65; (▼) Ref. 73. Data from mixtures in N$_2$: (○) Ref. 72; (△) Ref. 65; (▽) Ref. 73; Recommended data (—).

and co-workers indicates that the Wang and Lee data are affected by both the disturbance of the electron energy distribution of pure argon by the attaching gas and by the incomplete stabilization of the anions for the total pressure they used. Both of these effects will be less pronounced as the buffer gas becomes more complex, as is indeed seen from the comparison of the two sets of measurements in N$_2$ buffer gas shown in Fig. 19(b). The data of Christophorou and co-workers are preferred over those of Wang and Lee for both of these buffer gases, because they have lower uncertainties, were corrected for the effect of total pressure, and cover a much larger range of E/N. For the more complex buffer gas CH$_4$, these effects are expected to be significantly reduced, and the Wang and Lee data shown in Fig. 19(c) are expected to be least affected by the factors just discussed. Overall, the uncertainty in the measurements of Wang and Lee is about $\pm 20\%$ and that of Christophorou and co-workers is less than $\pm 10\%$.

6.2.3. $k_{a,t}(\langle\varepsilon\rangle)$

The measurements of $k_{a,t}$ made as a function of E/N using Ar and N$_2$ as buffer gases can be plotted as a function of the mean electron energy $\langle\varepsilon\rangle$. This is possible because the electron energy distribution functions for these buffer gases are known at each value of E/N at which measurements of $k_{a,t}$ were made and because the experimental conditions were such that the electron–energy distributions were characteristic of the buffer gas alone. The latter condition was certainly met in the studies by Hunter and Christophorou[72] and Spyrou and Christophorou[32] as was indicated in Secs. 6.2.2. and 6.2.3. Figure 20 shows the results on $k_{a,t}(\langle\varepsilon\rangle)$ plotted this way. The data for the buffer gases N$_2$ and Ar agree well. The data of Wang and Lee are lower, probably because they were not extrapolated to infinite total gas pressure. The data of Christophorou and co-workers plotted in Fig. 20 are the values of the total electron attachment rate constant (for "infinitely" dilute mixtures of C$_3$F$_8$ in Ar or N$_2$ buffer gases)
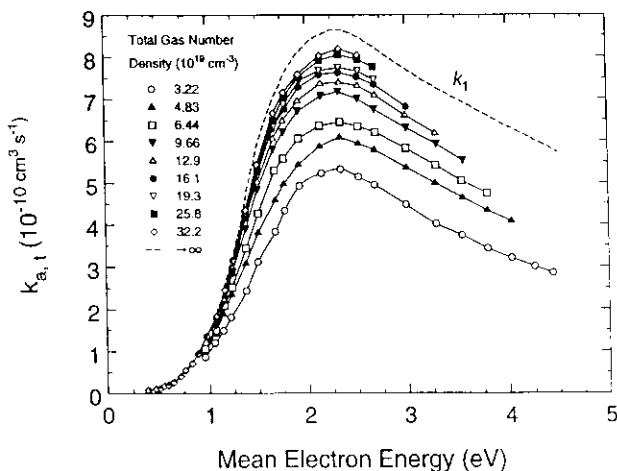
FIG. 21. Total electron attachment rate constant $k_{a,t}$ for C$_3$F$_8$ measured as a function of mean electron energy $\langle\varepsilon\rangle$ and total gas number density in a buffer gas of argon. The values of $k_{a,t}$ are those for infinitely dilute mixtures. The broken curve designated k_1 are the values of $k_{a,t}$ at "infinite" argon pressure, i.e., under conditions for which all transient C$_3$F$_8^{-*}$ ions can be stabilized by collision (from Ref. 72.)

extrapolated to "infinitely" large buffer gas density. Figure 21 shows an example of the dependence of $k_{a,t}(\langle\varepsilon\rangle)$ on the argon gas number density N_{Ar}. The values of $k_{a,t}(\langle\varepsilon\rangle)$ for $N_{Ar}\rightarrow\infty$ are shown in Fig. 21 by the curve designated k_1.

In Table 12 are listed the average values of the data in Fig. 20 excluding the measurements of Wang and Lee.[73] These represent our recommended values for the $k_{a,t}(\langle\varepsilon\rangle)$ ($T = 300$ K) of C$_3$F$_8$.

6.2.4. Thermal Value, $(k_{a,t})_{th}$, of the Total Electron Attachment Rate Constant

The thermal value, $(k_{a,t})_{th}$, of the total electron attachment rate constant of the C$_3$F$_8$ molecule is difficult to determine accurately due to the likely presence of traces of impurities which attach thermal electrons more efficiently than C$_3$F$_8$.

TABLE 12. Recommended total electron attachment rate constant, $k_{a,t}(\langle\varepsilon\rangle)$ ($T = 300$ K) for C$_3$F$_8$

Mean electron energy (eV)	$k_{a,t}(\langle\varepsilon\rangle)$ (10^{-10} cm^3 s^{-1})	Mean electron energy (eV)	$k_{a,t}(\langle\varepsilon\rangle)$ (10^{-10} cm^3 s^{-1})
0.05	0.02	1.75	7.64
0.07	0.02	2.00	8.42
0.10	0.02	2.25	8.65
0.20	0.02	2.50	8.50
0.30	0.02	2.75	8.20
0.40	0.03	3.00	7.84
0.50	0.07	3.25	7.54
0.60	0.15	3.50	7.16
0.70	0.28	3.75	6.80
0.80	0.50	4.00	6.44
0.90	0.85	4.25	6.10
1.00	1.54	4.50	5.74
1.25	3.80	4.75	5.45
1.50	6.10	...	...

TABLE 13. Measured thermal ($T=300$ K) values, $(k_{a,t})_{th}$, of the total electron attachment rate constant for C_3F_8

$(k_{a,t})_{th}$ (cm^3 s^{-1})	Reference
$<10^{-15}$	74
$\leqslant 3 \times 10^{-13}$	60
$<1.2 \times 10^{-12}$	75
1.8×10^{-12}	72

The possible presence of such impurities does not, however, affect the electron attachment measurements at higher energies because the magnitude of $k_{a,t}$ for C_3F_8 is much larger at higher energies than at thermal energies. The reported[60,72,74,75] measured values of $(k_{a,t})_{th}$ are listed in Table 13. They show that the $(k_{a,t})_{th}$ of C_3F_8 is small, less than about 1.8×10^{-12} cm^3 s^{-1}.

6.3. Total Electron Attachment Cross Section, $\sigma_{a,t}(\varepsilon)$ and Total Dissociative Electron Attachment Cross Section, $\sigma_{da,t}(\varepsilon)$

Since electron attachment to the C_3F_8 molecule is pressure dependent, care must be exercised to distinguish between the total electron attachment cross section $\sigma_{a,t}(\varepsilon)$ which is pressure dependent and the total *dissociative* electron attachment cross section $\sigma_{da,t}(\varepsilon)$ which is pressure independent. The former can be deduced from the total electron attachment rate constant measurements made in swarm experiments (Sec. 6.2.), and the latter normally from electron beam studies.

In Fig. 22(a) are shown two sets of values of the total electron attachment cross section $\sigma_{a,t}(\varepsilon)$ unfolded by Christophorou and collaborators[32,72] from their room temperature $k_{a,t}(\langle\varepsilon\rangle)$ data. The uncertainty of these cross sections is over $\pm 10\%$. The average of the two independent determinations of $\sigma_{a,t}(\varepsilon)$ is represented in Fig. 22(a) by the solid line. Values taken off this curve are given in Table 14 as our recommended values for the room temperature $\sigma_{a,t}(\varepsilon)$ of the C_3F_8 molecule.

In Fig. 22(b) is shown the total dissociative attachment cross section $\sigma_{da,t}(\varepsilon)$, deduced from swarm experiments by Spyrou and Christophorou[32] at $T=300$ K and the electron beam measurements of Chantry and Chen[33] at a somewhat higher temperature (330 K). Chantry and Chen[33] obtained their $\sigma_{da,t}(\varepsilon)$ cross section by normalization to the cross section data for the production of O^- from N_2O of Rapp and Briglia.[76] The $\sigma_{da,t}(\varepsilon)$ of Chantry and Chen has a value of 1.75×10^{-17} cm^2 at 2.8 eV. The agreement between the electron swarm and the electron beam data is reasonable considering the difference in temperature and technique. The average of the two sets of values for $\sigma_{da,t}(\varepsilon)$ is shown in Fig. 22(b) by the solid line. Data taken off this curve are listed in Table 15 as our recommended values for the $\sigma_{da,t}(\varepsilon)$ of the C_3F_8 molecule at about 300 K.

In addition to the data just discussed, there are three earlier measurements of $\sigma_{da,t}(\varepsilon)$ which vary by large factors from the more recent measurements and are not considered reli-
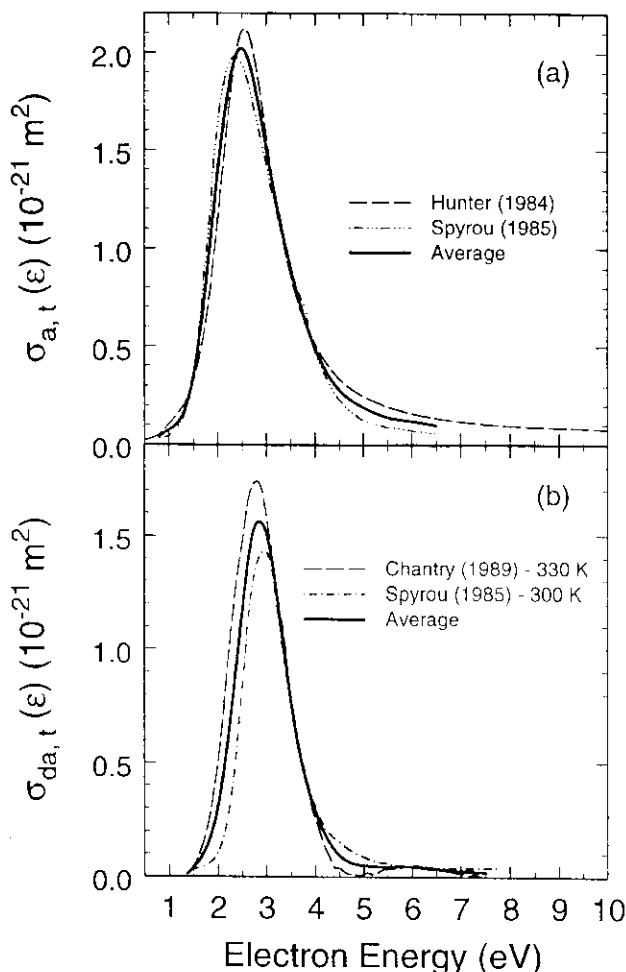
FIG. 22. (a) Total electron attachment cross section, $\sigma_{a,t}(\varepsilon)$, for C_3F_8 ($T=300$ K) unfolded from swarm data: (·······) Ref. 72; (--) Ref. 32; (—) average. (b) Total dissociative electron attachment cross section, $\sigma_{da,t}(\varepsilon)$, for C_3F_8: (-·-) swarm data of Spyrou and Christophorou (Ref. 32) at $T=300$ K; (--) beam data of Chantry and Chen (Ref. 33) at $T=330$ K; (—) average of the two sets of measurements.

able. The older of these measurements is by Bibby and Carter.[49] These workers reported observation of F$^-$, CF$_3^-$ and $C_2F_5^-$ ions with cross section maxima at, respectively, 3.0, 3.4, and 3.2 eV and peak cross section values, respectively, equal to 3.65×10^{-20}, 0.23×10^{-20}, and 0.27×10^{-20} m^2. The sum of these is 4.15×10^{-20} m^2. This value is about 26 times larger than the peak cross section value of

TABLE 14. Recommended total electron attachment cross section, $\sigma_{a,t}(\varepsilon)$ ($T=300$ K) for C_3F_8

Energy (eV)	$\sigma_{a,t}(\varepsilon)$ (10^{-21} m^2)	Energy (eV)	$\sigma_{a,t}(\varepsilon)$ (10^{-21} m^2)
0.8	0.04	3.0	1.51
1.0	0.07	3.5	0.90
1.5	0.35	4.0	0.49
1.7	0.70	4.5	0.28
2.0	1.39	5.0	0.19
2.3	1.92	5.5	0.14
2.5	2.02	6.0	0.12
2.7	1.90	6.5	0.10

TABLE 15. Recommended total dissociative electron attachment cross section, $\sigma_{da,t}(\varepsilon)$ ($T = 300$ K), for C$_3$F$_8$

Energy (eV)	$\sigma_{da,t}(\varepsilon)$ (10^{-21} m^2)	Energy (eV)	$\sigma_{da,t}(\varepsilon)$ (10^{-21} m^2)
1.4	0.02	4.0	0.29
1.8	0.15	4.5	0.10
2.0	0.31	5.0	0.05
2.3	0.78	5.5	0.05
2.5	1.16	6.0	0.05
2.7	1.49	6.5	0.04
3.0	1.51	7.0	0.03
3.5	0.77	7.5	0.02

FIG. 23. Relative intensity of fragment negative ions produced by electron impact on C$_3$F$_8$. (Data of Spyrou et al., Ref. 71; the data shown have been corrected by these workers for the finite width of the electron pulse using an unfolding technique.)

$\sigma_{da,t}(\varepsilon)$ in Fig. 22(b). The second earlier measurement is that of Kurepa[77] who observed two maxima in $\sigma_{da,t}(\varepsilon)$ at about 3.3 and 6.5 eV, with respective cross section values equal to 2.38×10^{-20} and 0.11×10^{-20} m^2. The peak cross section value at 3.3 eV is more than a factor of 10 higher than the maximum value of $\sigma_{da,t}(\varepsilon)$ in Fig. 22(b). The third measurement of $\sigma_{da,t}(\varepsilon)$ is that of Harland and Franklin[78] who found the cross section maximum for F and CF$_3^-$ at, respectively, (3.15 ± 0.1) eV and (3.65 ± 0.1) eV with cross section values at these energies equal to 0.5×10^{-21} m^2 and 0.05×10^{-21} m^2, respectively. The sum of these values $(0.55 \times 10^{-21}$ m$^2)$ is more than a factor of 3 lower than the value of $\sigma_{da,t}(\varepsilon)$ at 3.2 eV in Fig. 22(b).

6.4. Dissociative Electron Attachment Fragment Anions

There have been a number of studies on the identification, energetics, relative abundance, and energy dependence of the fragment negative ions formed in collisions of low energy electrons with the C$_3$F$_8$ molecule. The pertinent findings of these investigations[49,71,78,79] are summarized in Table 16. Bibby and Carter[49] observed F , CF$_3^-$, and C$_2$F$_5^-$ fragment anions using the electron impact method without improvement in the electron energy resolution. The appearance onsets of these fragment anions and the respective position of their maximum intensity are in reasonable agreement with the values of other researchers. Lifshitz and Grajower[79] used the retarding potential difference method (RPD) to improve the energy resolution of the electron beam and reported observation of F$^-$, F$_2^-$, CF$_3^-$, C$_2$F$_3^-$, C$_2$F$_5^-$ and C$_3$F$_7^-$. The peak positions and the energy thresholds for these ions are listed in Table 16. They are generally lower than the rest of the measurements. Harland and Franklin[78] reported thresholds and energies of maximum intensity for only F$^-$ and CF$_3^-$. Their values are within the combined experimental uncertainties of the other data.

The most recent and most complete study of negative ion formation by electron impact on C$_3$F$_8$ is that of Spyrou et al.[71] who also employed the RPD method to improve the electron beam energy resolution. They also employed an unfolding technique to correct the relative cross sections for the width of the electron pulse. Spyrou et al. observed five fragment anions from low energy electron impact on C$_3$F$_8$: F$^-$,
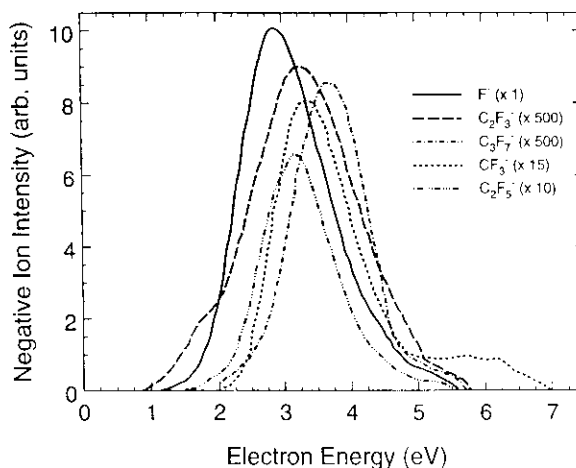
CF$_3^-$, C$_2$F$_3^-$, C$_2$F$_5^-$ and C$_3$F$_7^-$. Their energy onsets, energies of peak intensity, and relative abundances are given in Table 16 and they are in general agreement with the results of the other studies. The results of this study are shown in Fig. 23. The most significant anion is F produced by the breaking of C–F bonds (production of F$^-$ or C$_3$F$_7^-$) and the complementary anions CF$_3^-$ and C$_2$F$_5^-$ produced by the breaking of C–C bonds. The complementary ions CF$_3^-$ and C$_2$F$_5^-$ and the ion C$_2$F$_3^-$ have their resonance maxima at (3.3 ± 0.2) eV. The peak position of the predominant ion, F , and its weak complementary ion C$_3$F$_7^-$ are shifted to lower and higher energies, respectively, relative to the position of a common resonance at (3.3 ± 0.2) eV. There is evidence for a second resonance at energies > 5.5 eV.

Finally, Harland and Thynne[80] identified the fragment anions produced when 70 eV electrons interacted with C$_3$F$_8$. As expected, they observed more fragments than those produced at low energy by resonance electron attachment processes. Besides the ions listed in Table 16, they reported observation of a number of weaker (by factors of $\leqslant 10^{-4}$ compared to the intensity of F$^-$) anions: C , C$_2^-$, CF , C$_3^-$, F$_2^-$, C$_2$F$^-$, CF$_2^-$, C$_2$F$_2^-$, C$_3$F$_3^-$, and C$_3$F$_6^-$.

6.5. Effect of Temperature on $k_{a,t}(\langle \varepsilon \rangle)$ and $\sigma_{a,t}(\varepsilon)$

The temperature dependence of low-energy electron attachment processes in C$_3$F$_8$ is rather complicated, but understood. As can be seen from Fig. 24, the total electron attachment rate constant, $k_{a,t}(\langle \varepsilon \rangle)$, first decreases and then increases with increasing temperature above ambient. This is because low-energy electron attachment to C$_3$F$_8$ under swarm conditions leads to the formation of both parent and fragment negative ions. The rate constant for the former processes normally decreases with increasing gas temperature due to increasing autodetachment from the transient anion, and the rate constant for the latter processes normally increases with temperature due to increased autodissociation of

TABLE 16. Fragment negative ions produced by electron impact on C_3F_8, their energetics, and relative intensities

Fragment anion	Possible reaction	Energy threshold (eV)	Energy of maximum intensity (eV)	Relative abundance (Refs.)
F^-	$C_3F_8 + e \rightarrow F^- + C_3F_7$ [a]	1.7 ± 0.2	2.9 ± 0.1	100 (Ref. 71)
	$C_3F_8 + e \rightarrow F^- + n\text{-}C_3F_7$	2.0 ± 0.1	3.15 ± 0.1	— (Ref. 78)
	$C_3F_8 + e \rightarrow F^- + C_3F_7^*$	$\sim 4.0 \pm 0.1$		— (Ref. 78)
	$\rightarrow F^- + CF_3 + C_2F_4$			
	$\rightarrow F^- + CF_2 + C_2F_5$			
		1.8 ± 0.1	3.1 ± 0.1	100 (Ref. 80)
		4.1 ± 0.1		
		1.35 ± 0.1	~ 2.4	— (Ref. 79)
		1.8	3.0	— (Ref. 49)
CF_3^-	$C_3F_8 + e \rightarrow CF_3^- + C_2F_5$ [b,c]	2.4 ± 0.2	3.4 ± 0.1	5.4 (Ref. 71)
		> 5.0	> 5.5 [d]	
		2.55 ± 0.2	3.65 ± 0.1	— (Ref. 78)
		2.5 ± 0.1	3.6 ± 0.1	2.2 (Ref. 80)
		$> 5.2 \pm 0.1$	5.7 ± 0.1	— (Ref. 80)
		2.0 ± 0.1	~ 2.9	— (Ref. 79)
		2.2	3.4	— (Ref. 49)
$C_2F_5^-$		1.1 ± 0.1	3.3 ± 0.1	~ 0.2 (Ref. 71)
				< 0.01 (Ref. 80)
$C_2F_5^-$	$C_3F_8 + e \rightarrow C_2F_5^- + CF_3$ [b]	2.1 ± 0.2	3.2 ± 0.1	6.6 (Ref. 71)
		2.4 ± 0.1	3.4 ± 0.1	1.9 (Ref. 80)
		1.7 ± 0.1	~ 2.9	— (Ref. 79)
		2.1	3.2	— (Ref. 49)
$C_3F_7^-$		2.5 ± 0.2	3.75 ± 0.1	~ 0.2 (Ref. 71)
		2.9 ± 0.1	3.9 ± 0.1	0.03 (Ref. 80)
		2.4 ± 0.1	~ 3.2	— (Ref. 79)

[a]From their measurements on the energetics of this reaction, Spyrou et al. (Ref. 71) estimated the dissociation energy $D(F\text{-}C_3F_7)$ to be $\leq 5.15 \pm 0.2$ eV. This value is in very good agreement with the value $D(F\text{-}C_3F_7) \leq 5.2 \pm 0.1$ eV obtained earlier by Harland and Thynne (Ref. 80).

[b]From their measurements on the energetics of this reaction, Spyrou et al. (Ref. 71) estimated the dissociation energy $D(CF_3\text{-}C_2F_5)$ to be equal to 3.7 ± 0.2 eV.

[c]From their measurements on the energetics of this reaction Harland and Franklin (Ref. 78) estimated the dissociation energy $D(CF_3\text{-}C_2F_5)$ to be 4.6 ± 0.3 eV, and the electron affinity of the CF_3 radical to be 2.05 ± 0.2 eV.
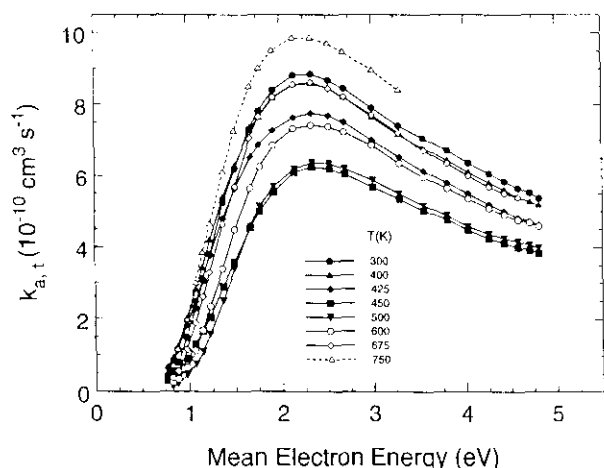
[d]Unresolved structure observed.

FIG. 24. Total electron attachment rate constant as a function of the mean electron energy, $k_{a,t}(\langle \varepsilon \rangle)$, for C_3F_8 measured at temperatures ranging from 300 to 750 K (data of Ref. 32). The data plotted were taken in mixtures of C_3F_8 with Ar and correspond to a very small pressure of C_3F_8 in a very large pressure of Ar, i.e., to the k_1 values shown in Fig. 21.

the transient anion.[81,82] In light of the data in Fig. 24 the total electron attachment cross section of the C_3F_8 molecule is expected to first decrease and then increase with increasing temperature above 300 K. This is indeed the case as can be seen from the data in Fig. 25. In Fig. 25(a) are plotted the data on the total electron attachment cross section $\sigma_{a,t}(\varepsilon)$ for temperatures (300–450 K) for which the cross section has a contribution from both parent and fragment anions. In Fig. 25(b) the cross sections plotted are only for dissociative attachment. The data shown for 300 K are the dissociative attachment part of the total electron attachment cross section at this temperature. The data for temperatures between 500 and 700 K are for the total dissociative attachment cross section $\sigma_{da,t}(\varepsilon)$ since at these temperatures there is no contribution to the cross section from the production of parent negative ions.[32]

Consistent with the swarm results in Fig. 25, are the electron beam measurements[33] on the formation of F^- by electron impact on C_3F_8 as a function of temperature shown in Fig. 26.
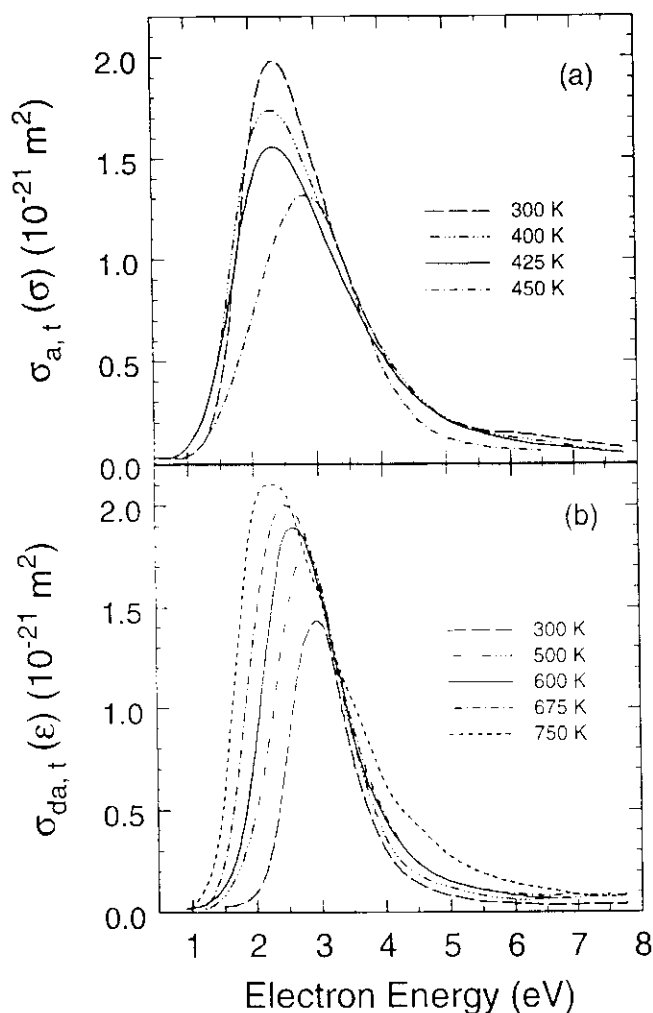
Fɪɢ. 25. Total electron attachment cross section. $\sigma_{a,t}(\varepsilon)$, for C_3F_8 unfolded by Spyrou and Christophorou (Ref. 32) from their $k_{a,t}((\varepsilon))$ data shown in Fig. 24 at (a) 300, 400, 425, and 450 K, and (b) 500, 600, 675, and 750 K. The 300 K data shown in the figure are the dissociative attachment part of the total electron attachment cross section at this temperature (data of Ref. 32).

Fɪɢ. 26. Cross section for the production of F⁻ by electron impact on C_3F_8 at gas temperatures of 300, 370, 510, and 730 K as measured in an electron beam experiment by Chantry and Chen (Ref. 33). For comparison the $\sigma_{da,t}(\varepsilon)$ for $T=750$ K from Fig. 25(b) is also shown in the figure.

6.6. Negative Ions in C₃F₈ Plasmas

Measurement of negative ion densities in rf plasmas of C_3F_8 have been made by Haverlag and co-workers[83] using laser photodetachment and subsequent detection of the photodetached electrons. Under their experimental conditions [13.56 MHz rf plasmas generated in a quasiparallel electrode system at pressures between 4 Pa (30 mTorr) and 16 Pa (120 mTorr) and power densities up to 0.25 W/cm²], they found the negative ion density to be more than a factor of 20 larger than the electron density. Such copious quantities of negative ions in the plasma may have origins other than the parent unexcited molecule. They most likely include fragment anions from electron attachment to radicals or from larger molecules formed by polymerization, or electron attachment to "hot" or electronically excited molecules or radicals for which dissociative attachment is normally significantly enhanced compared to the unexcited species.[81] Indeed, evidence for negative ion formation enhancement via these pro-
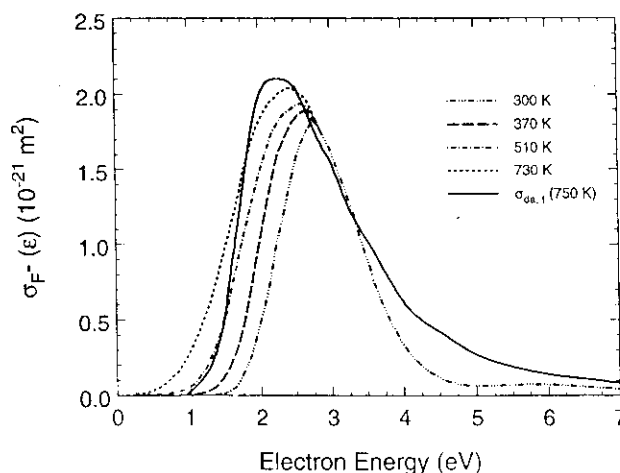
cesses in plasmas of CF_4 and CHF_3 has recently been obtained.[84] (See also a recent review on negative ions in low pressure discharges by Stoffels et al.[85])

In view of the increasing use of laser photodetachment to probe the negative ion concentrations in plasma reactors, measurement is indicated of the photodetachment cross sections of fragment anions for this molecule and also for other perfluorocarbon molecules of interest to plasma processing such as CF_4 and C_2F_6. Especially useful will be measurements of the photodetachment cross sections for the anions F^-, CF_2^-, CF_3^-, $C_2F_5^-$, and $C_3F_7^-$. The electron affinity [EA(F)] of the F atom is known. Although reported values of EA(F) range from 2.81 to 4.1 eV,[86] the values of (3.398 ±0.002) eV[87] and (3.400±0.002) eV[88] are considered the most accurate. The electron affinities of the other fragments are not well known. The values listed by Christodoulides et al.[86] vary considerably: 0.20–2.65 eV for CF_2, 1.36–2.60 eV for CF_3, 2.1–3.3 eV for C_2F_5, and 2.2–2.4 eV for C_3F_7.

7. Electron Transport

7.1. Electron Drift Velocity, w

There have been two measurements[45,89] of the electron drift velocity, w, in pure C_3F_8. These measurements are shown in Fig. 27 and are not in agreement. Naidu and Prasad[45] made their w measurements in the pressure range 0.08 kPa (0.6 Torr)–0.267 kPa (2 Torr) and at E/N values $(270\times10^{-21}-630\times10^{-21}$ V m² at $T=293$ K) relatively larger than those of Hunter et al.[89] $(0.4\times10^{-21}-500 \times10^{-21}$ V m²). Naidu and Prasad reported no effect of gas number density on w, with an overall uncertainty in their measurements of less than ±5%. Hunter et al.[89] employed a pulsed Townsend method and pressures in the range 0.5–3.0 kPa. The estimated total uncertainty in their w values when electron attachment and ionization are negligible is ±2%, but it rises to a maximum of ±5% when either the ionization or the attachment coefficient is large due mainly to an in-
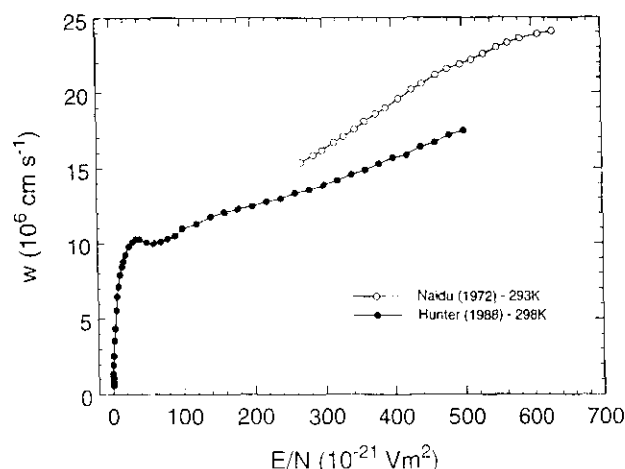
Fig. 27. Electron drift velocity, w, as a function of E/N in pure C₃F₈: (●) Ref. 89 (T = 298 K). (○) Ref. 45 (T = 293 K).

TABLE 17. Suggested electron drift velocities, w, in C_3F_8 ($T = 298$ K)[a]

E/N (10^{-21} V m^2)	w (10^6 cm s^{-1})	E/N (10^{-21} V m^2)	w (10^6 cm s^{-1})
0.40	0.60	80	10.3
0.50	0.75	90	10.5
0.60	0.88	100	11.0
0.80	1.14	120	11.3
1.0	1.39	140	11.8
1.5	1.98	160	12.1
2.0	2.57	180	12.3
3.0	3.57	200	12.5
4.0	4.37	220	12.8
6.0	5.57	240	13.0
8.0	6.49	260	13.4
10	7.14	280	13.6
12	7.92	300	13.9
15	8.45	320	14.2
17	8.80	340	14.6
20	9.25	360	14.9
25	9.8	380	15.3
30	10.1	400	15.7
35	10.3	420	15.9
40	10.3	440	16.4
50	10.1	460	16.7
60	10.0	480	17.2
70	10.1	500	17.5

[a]Data of Hunter et al., Ref. 89.

creased uncertainty in determining the electron transit time from the break in the voltage wave form. The temperature of their experiment was 298 K. Contrary to the conclusion of Naidu and Prasad that w is not a function of gas density, Hunter et al.[89] found that w depends on gas number density at high E/N even after allowing for nonequilibrium and boundary corrections to the measured electron swarm transit time. The largest pressure dependence of w occurs at E/N values near $(E/N)_{lim}$ ($\sim 290 \times 10^{-21}$ V m^2 at a gas pressure of 0.05 kPa). The pressure dependence of w decreases at lower E/N such that it becomes independent of gas pressure at $E/N < 150 \times 10^{-21}$ V m^2. Hunter et al. attributed these changes in w with the C_3F_8 pressure to the effect of electron attachment on the electron energy distribution function resulting from increases in the electron attachment coefficient with increasing gas density. The magnitude of the change in

w with pressure correlates with the magnitude of the change in the attachment coefficient with gas density for this molecule.

Hunter et al.[89] attributed the differences between their measurements and those of Naidu and Prasad[45] to the experimental uncertainties in the latter measurements. They pointed out that the determination of w made by Naidu and
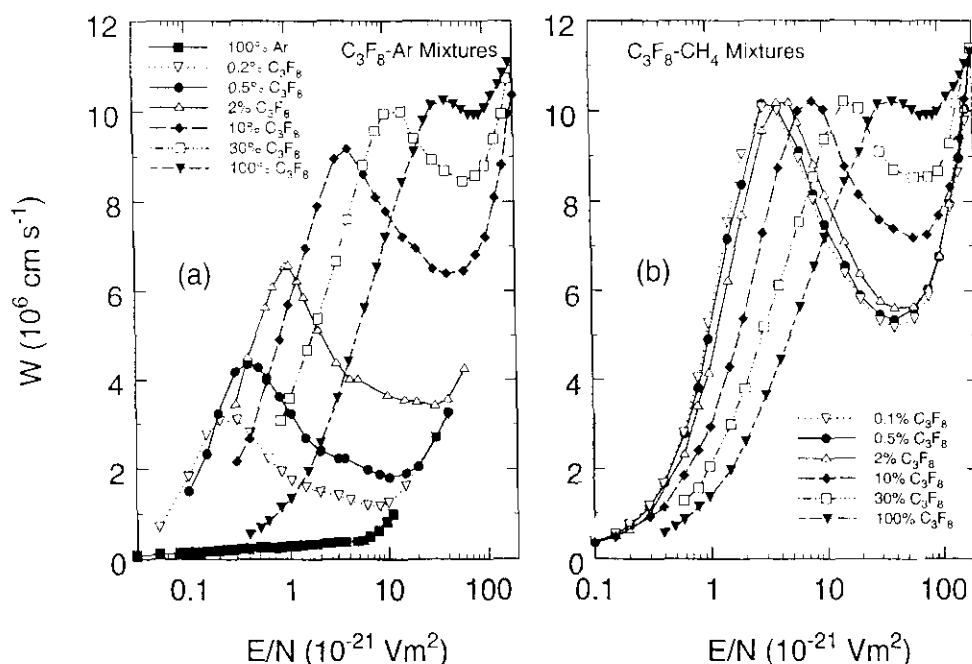

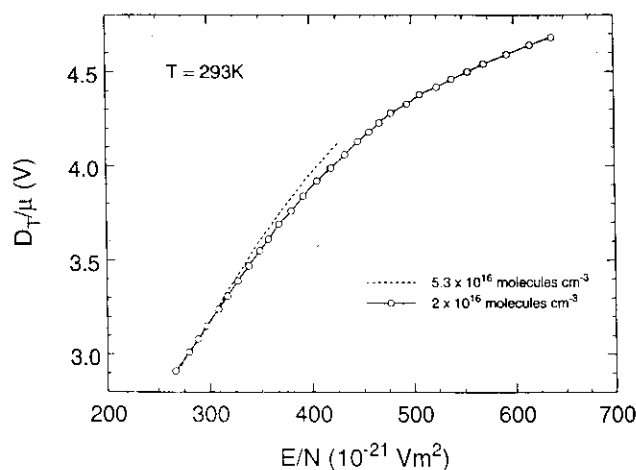Fig. 28. Electron drift velocity in (a) C₃F₈–Ar mixtures and (b) C₃F₈–CH₄ mixtures (data from Ref. 16).

FIG. 29. D_T/μ as a function of E/N for C_3F_8 ($T = 293$ K) (data from Ref. 45): (---) $N = 5.3 \times 10^{16}$ molecules cm^{-3}; (-O-) $N = 2.0 \times 10^{16}$ molecules cm^{-3}.

TABLE 18. Suggested D_T/μ values for C_3F_8 ($T = 293$ K) [a]

E/N (10^{-21} V m^2)	D_T/μ (V)	E/N (10^{-21} V m^2)	D_T/μ (V)
270	2.93	460	4.19
280	3.01	480	4.28
290	3.09	500	4.35
300	3.17	520	4.41
320	3.33	540	4.46
340	3.48	560	4.51
360	3.62	580	4.56
380	3.76	600	4.60
400	3.89	620	4.65
420	3.99	640	4.68
440	4.10		

[a]Data of Naidu and Prasad, Ref. 45, for a gas density of 2.0 $\times 10^{16}$ molecules cm^{-3}.

Prasad was limited by the finite width of the pulsed light source they used and by high background ion currents. Since, compared to the Prasad and Naidu data, the measurements of Hunter et al. have lower uncertainties, stretch over a wider range of E/N values, and are corrected for gas density and other factors, they are preferred and are listed in Table 17 as our suggested w values for pure C_3F_8. Interestingly, the measurements show a region of negative differential conductivity (decrease in w with increasing E/N) which is less pronounced for C_3F_8 than for CF_4 (Ref. 21) and C_2F_6.[24]

Measurements have also been made of the w in mixtures of C_3F_8 with various gases such as Ar[11,16] and CH_4.[16] These measurements were partially motivated by the development

of fast mixtures for use in gas pulse-power switches (Sec. 1). A sample of these data taken from Hunter et al.[16] is shown in Fig. 28. It is interesting to note the negative differential conductivity exhibited by these mixtures for certain E/N regions which depend on mixture composition. Recently, measurements of w in a few C_3F_8/Ar mixtures were made[39,90] for use in multi-term Boltzmann analysis to determine electron collision cross section sets. The transport coefficients for the mixtures serve as a sensitive probe of the consistency of the calculated cross section sets.

7.2. Ratio of Transverse Electron Diffusion Coefficient to Electron Mobility D_T/μ

The only known measurements of D_T/μ for C_3F_8 are those of Naidu and Prasad[45] shown in Fig. 29. These mea-
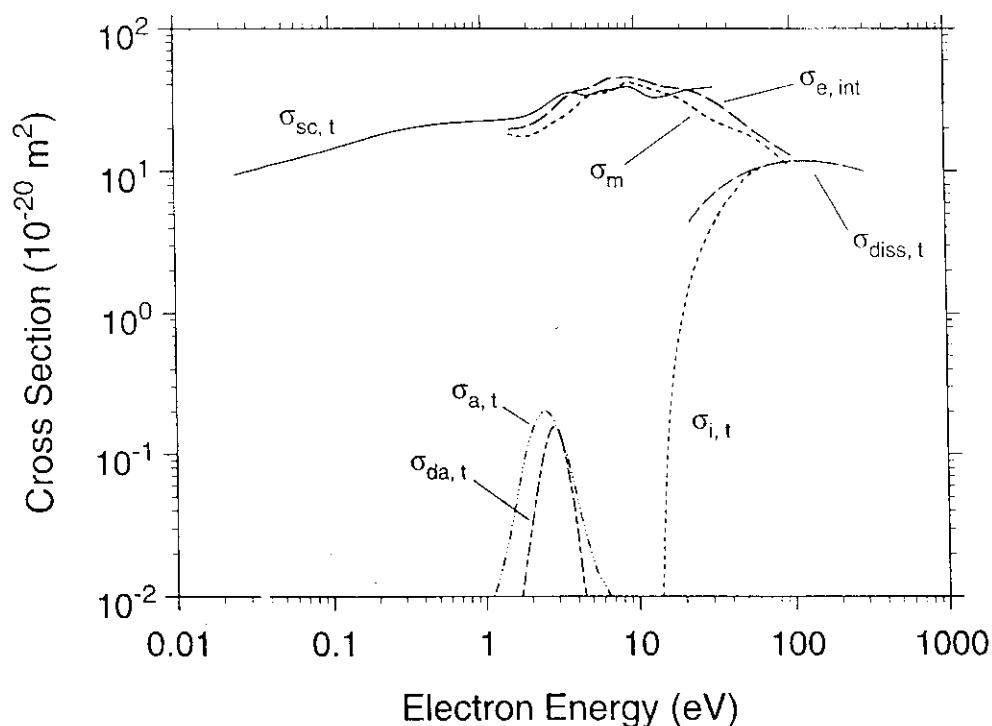

FIG. 30. Summary of recommended and suggested cross sections for C_3F_8 ($T = 298$ K).

surements were made at 293 K and have an overall reported uncertainty of about $\pm 5\%$. Interestingly, D_T/μ was observed to exhibit a small dependence on gas pressure. The measurements of Naidu and Prasad[45] for the gas density 2×10^{16} molecules cm^{-3} are listed in Table 18.

Recently, measurements were made of the product $D_L N$ (D_L is the longitudinal electron diffusion coefficient and N is the gas number density) as a function of E/N for specific mixtures of C_3F_8 in Ar (0.526%[39] and 5.05%[39,90]) for use in multi-term Boltzmann analysis to determine electron collision cross section sets. These transport coefficients along with w measurements for the same gas mixtures serve as a sensitive probe of the consistency of the calculated cross section sets.

8. Summary of Cross Sections and Coefficients

The cross sections that have been designated as recommended or suggested in this paper are plotted in Fig. 30. These include the recommended data of:

(i)   total ionization cross section, $\sigma_{i,t}(\varepsilon)$ in Table 8 (Fig. 9),

(ii) total dissociation cross section in Table 9 (Fig. 10),

(iii) total electron attachment cross section ($T=300$ K), $\sigma_{a,t}(\varepsilon)$ in Table 14 [Fig. 22(a)],

(iv) total dissociative electron attachment cross section ($T=300$ K), $\sigma_{da,t}(\varepsilon)$ in Table 15 [Fig. 22(b)], and

(v)   total electron scattering cross section, $\sigma_{sc,t}(\varepsilon)$ in Table 4 (Fig. 2).

They also include the suggested data of:

(i)   momentum transfer cross section, $\sigma_m(\varepsilon)$ in Table 5 (Fig. 3), and

(ii) integral elastic electron scattering cross section, $\sigma_{e,int}(\varepsilon)$ in Table 6 (Fig. 5).

The following coefficients are recommended:

(i)   density-reduced ionization coefficient, α/N in Table 10 (Fig. 11),

(ii) total electron attachment rate constant, $k_{a,t}$ for pure C_3F_8 of Hunter *et al.* (Fig. 18), and

(iii) total electron attachment rate constant, $k_{a,t}(\langle\varepsilon\rangle)$ in Table 12 (Fig. 20).

Also the following transport coefficients are suggested, in the absence of other data:

(i)   electron drift velocity, w, of Hunter et al.[89] in Table 17 (Fig. 27), and

(ii) ratio of transverse electron diffusion coefficient to electron mobility ratio, D_T/μ, of Naidu and Prasad[45] in Table 13 (Fig. 29).

While no values of the effective ionization or electron attachment coefficients are recommended or suggested here, because of the pressure dependence of these parameters, the data of Hunter *et al.*[60] are preferred.

Values of the recommended and suggested cross section and transport data are available on the World Wide Web at http://eeel.nist.gov/811/refdata.

9. Needed Data

With the exception of the electron attachment cross section, there is a need for further measurements on all other cross sections, especially for the cross sections for momentum transfer and integral elastic scattering (over an extended energy range), and vibrational excitation. There is also a need for a direct measurement of the dissociation cross section into neutrals. Measurements of the electron transport coefficients are also indicated.

10. Acknowledgments

11. References

[1] E. Kay, A. Dilks, and D. Seybold, J. Appl. Phys. **51**, 5678 (1980).

[2] C. Bubeck and E. Kay, J. Vac. Sci. Technol. **18**, 360 (1981).

[3] R. d'Agostino, F. Cramarossa, V. Colaprico, and R. d'Ettole, J. Appl. Phys. **54**, 1284 (1983).

[4] M. Haverlag, A. Kono, D. Passchier, G. M. W. Kroesen, W. J. Goedheer, and F. J. de Hoog, J. Appl. Phys. **70**, 3472 (1991).

[5] Y. Haque and B. D. Ratner, J. Polym. Sci.: Part B: Polym. Phys. **26**, 1237 (1988).

[6] L. Zazzera, W. Reagen, and A. Cheng, J. Electrochem. Soc. **144**, 3597 (1997).

[7] J. T. Houghton, L. G. Meira Filho, B. A. Callander, N. Harris, A. Kattenberg, and K. Maskell. "Climate Change 1995," *The Science of Climate Change* (Cambridge University Press, New York, 1996), p. 22.

[8] Intergovernmental Panel on Climate Change (IPCC). The 1994 Report of the Scientific Assessment Working Group of IPCC, p. 28.

[9] A. R. Ravishankara, S. Solomon, A. A. Turnipseed, and R. F. Warren, Science **259**, 194 (1993).

[10] C. M. Roehl, D. Boglu, C. Brhl, and G. K. Moortgat, Geophys. Res. Lett. **22**, 815 (1995).

[11] L. G. Christophorou, S. R. Hunter, J. G. Carter, and R. A. Mathis, Appl. Phys. Lett. **41**, 147 (1982).

[12] P. Bletzinger, in XVI International Conference on Phenomena in Ionized Gases, Contributed Papers, Vol. 2, edited by W. Bötticher, H. Wenk, and E. Schulz-Gulde, Duesseldorf, Germany, August 29–September 2, 1983, p. 218.

[13] L. G. Christophorou and S. R. Hunter, in *Electron Molecule Interactions and Their Applications*, edited by L. G. Christophorou (Academic, New York, 1984), Vol. 2, Ch. 5.

[14] S. R. Hunter, J. G. Carter, L. G. Christophorou, and V. K. Lakdawala, in *Gaseous Dielectrics IV*, edited by L. G. Christophorou and M. O. Pace (Pergamon, New York, 1984), p. 224.

[15] W. W. Byszewski, M. J. Enright, and J. M. Proud, in *Gaseous Dielectrics IV*, edited by L. G. Christophorou and M. O. Pace (Pergamon, New York, 1984), p. 255.

[16] S. R. Hunter, J. G. Carter, and L. G. Christophorou, J. Appl. Phys. **58**, 3001 (1985).

[17] L. G. Christophorou, D. L. McCorkle, and S. R. Hunter, in *Gaseous Dielectrics V*, edited by L. G. Christophorou and D. W. Bouldin (Pergamon, New York, 1987), p. 381.

[18] G. Camilli, T. W. Liao, and R. E. Plump, Trans. AIEE **74**, 637 (1955).

[19] L. G. Christophorou, R. A. Mathis, S. R. Hunter, and J. G. Carter, J. Appl. Phys. **63**, 52 (1988).

[20] L. G. Christophorou, Nucl. Instrum. Methods Phys. Res. A **268**, 424 (1988).

[21] L. G. Christophorou, J. K. Olthoff, and M. V. V. S. Rao, J. Phys. Chem. Ref. Data **25**, 1341 (1996).

[22] L. G. Christophorou, J. K. Olthoff, and M. V. V. S. Rao, J. Phys. Chem. Ref. Data **26**, 1 (1997).

[23] L. G. Christophorou, J. K. Olthoff, and Y. Wang, J. Phys. Chem. Ref. Data **26**, 1205 (1997).

[24] L. G. Christophorou and J. K. Olthoff, J. Phys. Chem. Ref. Data **27**, 1 (1998).

[25] J. A. Beran and L. Kevan, J. Phys. Chem. **73**, 3860 (1969).

[26] C. J. Noutary, J. Res. Natl. Bur. Stand. **72A**, 479 (1968).

[27] M. B. Robin, *Higher Excited States of Polyatomic Molecules* (Academic, New York, 1974), Vol. 1, pp. 178–191.

[28] G. Bélanger, P. Sauvageau, and Sandorfy, Chem. Phys. Lett. **3**, 649 (1969).

[29] M. J. S. Dewar and S. D. Worley, J. Chem. Phys. **50**, 654 (1969).

[30] C. Lifshitz and F. A. Long, J. Phys. Chem. **69**, 3746 (1965).

[31] I. Ishii, R. McLaren, A. P. Hitchcock, K. D. Jordan, Y. Choi, and M. B. Robin, Can. J. Chem. **66**, 2104 (1988).

[32] S. M. Spyrou and L. G. Christophorou, J. Chem. Phys. **83**, 2829 (1985).

[33] P. J. Chantry and C. L. Chen, J. Chem. Phys. **90**, 2585 (1989).

[34] H. F. Winters and M. Inokuti, Phys. Rev. A **25**, 1420 (1982).

[35] H. U. Poll and J. Meichsner, Contrib. Plasma Phys. **27**, 359 (1987).

[36] J. E. Sanabia, G. D. Cooper, J. A. Tossell, and J. H. Moore, J. Chem. Phys. **108**, 389 (1998).

[37] T. Shinohara, Y. Tachibana, M. Yuri, H. Tanaka, and L. Boesten, in Proceedings of the International Conference on the Physics of Electronic and Atomic Collisions, Whistler, British Columbia, Canada, 26 July–1 August 1995; Abstracts of Contributed Papers, edited by J. B. A. Mitchell, J. W. McConkey, and C. E. Brion, p. 13.

[38] H. Tanaka (private Communication, 1997).

[39] B.-H. Jeon and Y. Nakamura, paper presented at the International Conference on Atomic and Molecular Data and their Applications, September 29–October 2, 1997 (National Institute of Standards and Technology, Gaithersburg, MD), Paper MO35; Book of Abstracts, p. 45; private communication (October 1997).

[40] P. Pirgov and B. Stefanov, J. Phys. B **23**, 2879 (1990).

[41] C. Lifshitz and R. Grajower, Int. J. Mass Spectrom. Ion Phys. **4**, 92 (1970).

[42] L. G. Christophorou, *Atomic and Molecular Radiation Physics* (Wiley-Interscience, New York, 1971), Ch. 5.

[43] R. Merz and F. Linder (private communication, 1997).

[44] A. Mann and F. Linder, J. Phys. B **25**, 533 (1992).

[45] M. S. Naidu and A. N. Prasad, J. Phys. D **5**, 983 (1972).

[46] H. B. Milloy, R. W. Crompton, J. A. Rees, and A. J. Robertson, Aust. J. Phys. **30**, 61 (1977).

[47] F. E. Spencer and A. V. Phelps, *Proc. 15th Symp. Engineering Aspects of Magnetohydrodynamics* (University of Pennsylvania Press, Philadelphia, PA, 1976), p. IX.9.1.

[48] M. E. Riley, C. J. MacCallum, and F. Biggs, At. Data Nucl. Data Tables **15**, 443 (1975); Erratum **28**, 379 (1983).

[49] M. M. Bibby and G. Carter, Trans. Faraday Soc. **59**, 2455 (1963).

[50] J. A. Beran and L. Kevan, J. Phys. Chem. **73**, 3866 (1969).

[51] D. Rapp and P. Englander-Golden, J. Chem. Phys. **43**, 1464 (1965).

[52] H. Nishimura, W. M. Huo, M. A. Ali, and Y.-K. Kim, J. Chem. Phys. (submitted); Dr. Y.-K. Kim (private communication, 1998).

[53] Y.-K. Kim and M. E. Rudd, Phys. Rev. A **50**, 3954 (1994).

[54] W. Hwang, Y.-K. Kim, and M. E. Rudd, J. Chem. Phys. **104**, 2956 (1996).

[55] S. Motlagh and J. H. Moore, J. Chem. Phys. **109**, 432 (1998).

[56] R. Hermann, Radiat. Phys. Chem. **34**, 369 (1989).

[57] N. P. Danilevskii, I. Yu. Rapp, V. T. Koppe, and A. G. Koval, Opt. Spectrosc. (USSR) **60**, 441 (1986).

[58] M.-M. Chen and Y. H. Lee, Proc. Electrochem. Soc. **83**, 3 (1983).

[59] J. L. Moruzzi and J. D. Craggs, Proc. Phys. Soc. **82**, 979 (1963).

[60] S. R. Hunter, J. G. Carter, and L. G. Christophorou, J. Chem. Phys. **86**, 693 (1987).

[61] J. W. Gallagher, E. C. Beaty, J. Dutton, and L. C. Pitchford, J. Phys. Chem. Ref. Data **12**, 109 (1983).

[62] G. Biasiutti, in *Gaseous Dielectrics III*, edited by L. G. Christophorou (Pergamon, New York, 1982), p. 174.

[63] K. Nakanishi, D. R. James, H. Rodrigo, and L. G. Christophorou, J. Phys. D **17**, L73 (1984).

[64] R. E. Wootton, S. J. Dale, and N. J. Zimmerman, in *Gaseous Dielectrics II*, edited by L. G. Christophorou (Pergamon, New York, 1980), p. 137.

[65] S. R. Hunter, L. G. Christophorou, D. R. James, and R. A. Mathis, in *Gaseous Dielectrics III*, edited by L. G. Christophorou (Pergamon, New York, 1982), p. 7.

[66] S. R. Hunter and L. G. Christophorou, J. Appl. Phys. **57**, 4377 (1985).

[67] S. R. Hunter and L. G. Christophorou, in *Gaseous Electronics IV*, edited by L. G. Christophorou and M. O. Pace (Pergamon, New York, 1984), p. 115.

[68] L. G. Christophorou, R. A. Mathis, S. R. Hunter, and J. G. Carter, in *Gaseous Dielectrics V*, edited by L. G. Christophorou and D. W. Bouldin (Pergamon, New York, 1987), p. 88.

[69] G. F. Reinking, L. G. Christophorou, and S. R. Hunter, J. Appl. Phys. **60**, 499 (1986).

[70] K. Nakanishi, L. G. Christophorou, J. G. Carter, and S. R. Hunter, J. Appl. Phys. **58**, 633 (1985).

[71] S. M. Spyrou, I. Sauers, and L. G. Christophorou, J. Chem. Phys. **78**, 7200 (1983).

[72] S. R. Hunter and L. G. Christophorou, J. Chem. Phys. **80**, 6150 (1984).

[73] W. C. Wang and L. C. Lee, J. Appl. Phys. **58**, 184 (1985).

[74] R. W. Fessenden and K. M. Bansal, J. Chem. Phys. **53**, 3468 (1970).

[75] F. J. Davis, R. N. Compton, and D. R. Nelson, J. Chem. Phys. **59**, 2324 (1973).

[76] D. Rapp and D. D. Briglia, J. Chem. Phys. **43**, 1480 (1965).

[77] M. V. Kurepa, *3rd Czechoslovakian Conference on Electronics and Vacuum Physics Transactions*, Prague, September 23–28, 1965 (1967), p. 107.

[78] P. W. Harland and J. L. Franklin, J. Chem. Phys. **61**, 1621 (1974).

[79] C. Lifshitz and R. Grajower, Int. J. Mass Spectrom. Ion Phys. **3**, 211 (1969).

[80] P. W. Harland and J. C. J. Thynne, Int. J. Mass Spectrom. Ion Phys. **9**, 253 (1972).

[81] L. G. Christophorou, L. A. Pinnaduwage, and P. G. Datskos, in *Linking the Gaseous and Condensed Phases of Matter*, edited by L. G. Christophorou, E. Illenberger, and W. Schmidt (Plenum, New York, 1994), p. 415.

[82] L. G. Christophorou and P. G. Datskos, Int. J. Mass Spectrom. Ion Proc. **149/150**, 59 (1995).

[83] A. Kono, M. Haverlag, G. M. W. Kroesen, and F. J. de Hoog, J. Appl. Phys. **70**, 2939 (1991).

[84] W. W. Stoffels, E. Stoffels, and K. Tachibana, Jpn. J. Appl. Phys., Part 1 **36**, 4638 (1997).

[85] E. Stoffels, W. W. Stoffels, D. Vender, M. Haverlag, G. M. W. Kroesen, and F. J. de Hoog, Contrib. Plasma Phys. **35**, 331 (1995).

[86] A. A. Christodoulides, D. L. McCorkle, and L. G. Christophorou, in *Electron Molecule Interactions and their Applications*, edited by L. G. Christophorou (Academic, New York, 1984), Vol. 2, Ch. 6.

[87] R. Milstein and R. S. Berry, J. Chem. Phys. **55**, 4146 (1971).

[88] H.-P. Popp, Z. Naturforsch. A **20**, 642 (1965).

[89] S. R. Hunter, J. G. Carter, and L. G. Christophorou, Phys. Rev. A **38**, 58 (1988).

[90] B.-H. Jeon, S.-C. Ha, and Y. Nakamura, Proceedings of the XXIII International Conference on Phenomena in Ionized Gases, Contributed Papers, edited by M. C. Bordage and A. Gleizes, 17–22 July, Toulouse, France, Vol. 5, p. V-4.